AN ABSTRACT OF THE THESIS OF

Youcef Yahiaoui for the degree of Master of Science in Electrical and Computer Engineering presented on June 7, 1999. Title: Bilinear System Model of the Action Potential of a Single Neuron

Abstract approved: _____

R. R. Mohler

Neurons are characterized by an electric potential which is established between their inside and outside media. They exhibit specific voltage fluctuations, in response to strong enough current impulses, called action potentials.

In this work, a bang-bang controlled bilinear system (BLS) is derived to approximate the generation of a simple neuron's action potential. The shape of the response, as well as the timing seem to be useful for experimental planning and interpretation to neural physiologists. The BLS-model has the potential to aid the design and fabrication of commercial neural networks for communication, control and computing.

In this manner, a variable-structure membrane impedance, such as exhibited by a stable focus and a saddle point in state space, and/or other modes, arises naturally. Added positive and negative stimuli, such as from other neurons, have the capability to alter the voltage across the inside and the outside media of the neuron and elicit an advanced or delayed response in the action potential. Such latency is significant as noted above, and is an active area of experimental research.

The response shape and the timing with respect to some other event(latency) are related to experimental data. This simple model is compared to the complex and highly celebrated Hodgkin-Huxley model for the squid giant axon. The bang-bang feedback control is given a biological interpretation of sodium and potassium ion channels in this axon, that yields a variable-structure membrane impedance.

Bilinear System Model of the Action Potential of a Single Neuron.

by

Youcef Yahiaoui

A THESIS

submitted to

Oregon State University

in partial fulfillment of
the requirements for the
degree of

Master of Science

Completed June 7, 1999
Commencement June 2000

Master of Science thesis of Youcef Yahiaoui presented on June 7, 1999

APPROVED:

Redacted for Privacy

Major Professor, representing Electrical and Computer Engineering

Redacted for Privacy

Chair of the Department of Electrical and Computer Engineering

Redacted for Privacy

Dean of the Graduate School

I understand that my thesis will become part of the permanent collection of Oregon State University libraries. My signature below authorizes release of my thesis to any reader upon request.

Redacted for Privacy

Youcef Yahiaoui, Author

ACKNOWLEDGMENT

This work has been done at the Oregon State University in the Electrical and Computer Engineering Department. It came together with the help of many talented and supportive people.

Special thanks to both Professor R. Mohler and Professor G. Mpitsos for their guidance and their continuous help and advice. I am also indebted to Professor M. Shor and V. Stonick who provided me with help whenever I asked for it. I am very happy to express my gratitude to all the ECE Professors for all I learned from them and for their perseverance and dedication.

I can not forget to direct my special thanks to the ECE administration staff for their good care and attention to the students.

Finally, I am grateful for the partial support of this research by NSF Grant No. 9530917.

TABLE OF CONTENTS

Page

1. SOME BASIC NEUROBIOLOGY 1
   - 1.1. Introduction 1
   - 1.2. The Classical Neuron 2
   - 1.3. Neural Electrical Behavior 4
     - 1.3.1. *The Membrane Potential* 4
     - 1.3.2. *Hyperpolarization* 5
     - 1.3.3. *Depolarization* 5

2. SOME MATHEMATICAL MODELS OF NEURONS 7
   - 2.1. Introduction 7
     - 2.1.1. *Membrane Impedance* 7
     - 2.1.2. *Nernst's Equation* 8
     - 2.1.3. *Direct Measurement of Ionic Currents in Axon Membranes* 9
     - 2.1.4. *Voltage-Clamp Method* 9
   - 2.2. Hodgkin and Huxley(HH) Model 11
     - 2.2.1. *Hodgkin and Huxley Conventions* 12
     - 2.2.2. *Ionic Currents* 13
     - 2.2.3. *HH-model Equations* 16

3. A SIMPLE BANG-BANG CONTROLLED BILINEAR MODEL 17
   - 3.1. Introduction 17
   - 3.2. Background on Second Order Systems 19
     - 3.2.1. *Stable Focus* 20
     - 3.2.2. *Saddle Point* 20
   - 3.3. Neuron Properties 24
     - 3.3.1. *Pulse Timing* 24
     - 3.3.2. *I/O properties of single Neurons* 24
   - 3.4. Inductance Effect in the Ionic Channel 27
     - 3.4.1. *Inductive feature of a neuron membrane* 27
     - 3.4.2. *General Model of an Ionic Channel* 27
     - 3.4.3. *Latency Experiments on a Simple Second-Order System* 30

4. SINGLE NEURON MODEL 32
   - 4.1. Introduction 32
   - 4.2. Refractoriness 32

TABLE OF CONTENTS (Continued)

Page

4.3. Threshold Determination 32
4.4. Results 35
4.5. Coefficient Determination Based on The HH-Action Potential 36
4.5.1. *Stable Focus* 36
4.5.2. *Saddle Point* 38
4.6. Model Parameter Identification 40
4.6.1. *Recursive Parameter Identification Using RPM/RLS* 40
4.6.2. *Optimal Parameter Determination of the Coefficients in the Three Spike Regions.* 42
4.6.3. *Estimated Parameter Values* 45

5. CONCLUSION AND PERSPECTIVE 49

BIBLIOGRAPHY 53

APPENDICES 56
A Continuous System Identification 57
B Latency Curves From a Stable Focus System with a Lead Term 72
C Simulink Model of Hodgkin and Huxley Equations 79
D Simulink Implementation of the BLS-model with Dual Stable focus Equilibrium Points 80

LIST OF FIGURES

Figure		Page
1.1	Generic neuron cell	3
1.2	The synapse	4
1.3	A microelectrode used to measure the electric properties of a cell.	5
1.4	Electrical response of the neuron to stimulation[2]	6
1.5	Electrical response of the neuron to stimulation[2]	6
2.1	Membrane conductance increase during propagated action potential. Time course of the action potential is given by the dotted line for comparison. (From Cole & Curtis[3])	8
2.2	Three Voltage-clamp methods[4]	10
2.3	Recorded voltage-clamp currents with a hyperpolarizing and depolarizing pulses. ([4],ch4, page109).	11
2.4	Separation of ionic currents in squid giant axon by ionic substitution method. ([4],ch4, page110).	12
2.5	Hodgkin and Huxley model equivalent circuit	13
3.1	Voltage spike and m, h and n variations during the excitation of HH model with a short current impulse.	18
3.2	Sodium and Potassium conductances—HH model— versus time during the spiking.	19
3.3	a and b regions for stable node and saddle point	21
3.4	State space representation of the switching process	22
3.5	Spike obtained from the bilinear system	23
3.6	Perturbation of a neuron cell by hyperpolarizing and depolarizing impulses[5]	25
3.7	Three superimposed simulation sweeps[5]	26
3.8	Latency (I/O) curve shapes[5]	26
3.9	Impedance plots of a neuron membrane under subthreshold conditions. They are obtained by simulations of HH-model[5]	28
3.10	Equivalent circuit of a membrane channel.	29

LIST OF FIGURES (Continued)

Figure		Page
3.11	Latency simulations	30
3.12	Depolarization and Hyperpolarization latency curves. A_i are the amplitudes of the perturbing impulses.	31
4.1	Block diagram of the Switching circuit	34
4.2	Phase plot illustration	35
4.3	Time trajectories of the model output for different input frequencies	36
4.4	HH-spike used for a rough parameter determination.	38
4.5	Comparison of the HH-spike and that produced by a bilinear system(fit not optimized)	39
4.6	HH-neuron input and output for identification.	41
4.7	Identified four parameters throughout the spiking process using RPM/RLS method.	42
4.8	HH-neuron spike divided into three piecewise constant parameter regions.	43
4.9	Superposition of the HH-spike with the reconstructed version using optimally determined parameters.	46

LIST OF FIGURES (Continued)

Figure Page

LIST OF APPENDIX FIGURES

5.1 Output model of a system H(s) 58

5.2 Variance of the estimation error vs K[6] 59

5.3 Mobile horizon in the reinitialized partial moment computation.[6] 60

5.4 Simulation set-up for system identification 63

5.5 Step input with a PRBS and the system output 64

5.6 The 4 identified parameters. 65

5.7 Output reconstructed using the identified parameters. It is superposed on the original contaminated output signal. 66

5.8 Latency Simulation Setup 72

5.9 Simulation Parameters: Solver 74

5.10 Simulation Parameters: Workspace. 75

5.11 Simulation relay block 76

5.12 Simulation Pulse Generator(Input Primary Pulse): 77

5.13 Simulation Pulse Generator1 78

5.14 Simulink implementation of the HH-model 79

5.15 Simulink implementation of the BLS Model 80

LIST OF TABLES

Table — Page

4.1 Optimal parameters for curve fitting the action potential in three regions .. 45

4.2 Control variables for changing the membrane structure during the spiking process. 47

LIST OF APPENDIX FIGURES

Figure **Page**

5.1 Output model of a system H(s) 58
5.2 Variance of the estimation error vs K[6] 59
5.3 Mobile horizon in the reinitialized partial moment computation[6] 60
5.4 Simulation set-up for system identification 63
5.5 Step input with a PRBS and the system output 64
5.6 The 4 identified parameters 65
5.7 Output reconstructed using the identified parameters. It is superposed on the original contaminated output signal 66
5.8 Latency Simulation Set-up 72
5.9 Simulation Parameters: Solver 74
5.10 Simulation Parameters: Workspace 75
5.11 Simulation relay block 76
5.12 Simulation Pulse Generator (Input Primary Pulse) 77
5.13 Simulation Pulse Generator1 78
5.14 Simulink implementation of the HH-model 79
5.15 Simulink implementation of the BLS-model 80

To my wife Lorna and My new son Jesse Voujemaa,

With love to my mother, to my brothers and sister Rosa,

To my new baby niece Ania and her parents,

In the memory of my father and my grandmas Thawaamarats and Setsihwa.

To all those who militate in favour of freedom, love, peace and progress in the world.

OBJECTIVE OF THE THESIS

The objective of this work is to model the electrical behavior of a single neuron. This work is based on using piecewise linear systems combined through switching into what is commonly called bilinear system (BLS). The model is compared to the Hodgkin-Huxley (HH) model [1] and should implement two features which seem to be important in the biological nature of the communication between nerve cells as well as produce the temporal shape of the the neuron action potential. One of these features is the natural insensitivity to inputs while the neuron is in the process of firing—spiking—after being excited. This is referred to as the neuron refractoriness. The sensitivity progressively regenerates during the settling of the neuron's voltage around its resting potential.

The second feature is related to the effect different perturbing excitations, distributed in time, have on the timing of an action potential. Here, the cell's voltage is driven to a point where an action potential is produced by a just strong enough input current, the time of which also defines a reference for subsequent spike occurrences. Depending on the amplitudes, the relative time positions, and the presentation time of different perturbing excitations presented to a neuron in conjunction with the reference input current, the voltage of this reaches the firing level—threshold—at different times (latency) accordingly.

The complexity of HH-model makes it very difficult to perform any analysis on it because the coefficients of its first order differential equation themselves are solutions of another set of coupled first order differential equations of quantities raised to different powers.

It seems that switching between piecewise linear systems having different equilibrium points can provide enough flexibility to generate a model which would satisfy the features mentioned above. This would benefit from the technology of intergration of electronic circuits (switching circuits) and from its simplicity to build neuron models that would link biologists and engineers as to what is happening to the neuron membrane at rest or during activation.

PREFACE

This work is organized into five main chapters. The first chapter provides a brief biological description of a neuron and its different constituent elements. It introduces the electrical behavior of the neuron membrane.

The second chapter covers the concept of the membrane selective permeability to different ions in light of the types of the involved ions. This chapter contains three main parts: the first of which deals with the fundamentals of the membrane theory and the description of the membrane potentials. The second part presents different means used to measure the different membrane currents which are the bases in the development of the Hodgkin and Huxley model for the squid giant axon. The third part describes the HH-model itself.

After a brief review of second-order systems, the third chapter briefly mentions the inductance equivalent effect from average impedance plots obtained from simulations of the HH-model. This chapter ends by some latency curves carried out on a second-order system characterized by a stable focus as its equilibrium point and having a lead term noted in the impedance plots.

Chapter four presents the bang-bang bilinear model which is built step by step in order to satisfy some different features that real neurons (e.g. squid giant axon) exhibit. Two important features discussed here are refractoriness and latency. The absolute refractoriness translates the duration of complete insensitivity of the neuron to the incoming input current stimuli while its in the process of producing an action potential. Relative refractoriness, however, refers to the period which follows the absolute refractoriness during which this sensitivity is progressively recovered. To start with, a bilinear system is built to show the possibility to regenerate the spike shape by switching between two linear systems characterized by different types of equilibrium points. The two systems interpret the state of the membrane impedance depending on the voltage across it and its derivative.

On one hand, a saddle point is used to represent the sudden increase of the membrane action potential after a current excitation is applied. A stable focus,on the other hand, is used to model the fall of the membrane potential after this has reached the switching level.

Later in this chapter, it is shown that adding another stable focus to account for the sudden variation in the dynamics towards the tail of the spike helps improve the precision with which the HH-model spike is approximated.

Finally, chapter five concludes this work with a conclusion, comments and some perspectives. Appendix A outlines a tool which transforms a constant coefficient linear differential equation into a linear integral equation. This latter is suitable for use with a recursive least square method (RLS) in order to estimate the model parameters when the input and the output are collected from a real neuron. Some useful matlab codes and simulink models are also included in the Appendix.

Bilinear System Model of the Action Potential of a Single Neuron

1. SOME BASIC NEUROBIOLOGY

1.1. Introduction

Neuron or nerve cells are the elementary computing units of the nervous systems. The mammalian brain contains lots of them. The human brain contains between 10^{10} to 10^{11} neurons perhaps more being able to cooperate in an effective way. Some neurons in the human brain receive on the order of hundreds to thousands of connections from other neurons, making about 10^{15} connections. This number is much smaller than the number that would result if each cell is to be connected with every other cell.

Other types of cells also exist in the nervous system. Glia (glue) cells, which are known to perform important support functions, are the most common of these cells.

Neurons being highly mechanically sensitive (they respond to pressure), the central nervous system is mechanically protected by extraordinary means. The brain is encased in a hard skull. Since soft tissue can easily be damaged by being in contact with hard bone, the brain is floated in a cerebrospinal fluid, which provides a hydraulic suspension system. Neurons are metabolically very active. The human nervous system consumes about 25% of the body's energy. Being only 1% to 2% of the body weight, it requires more energy than any other tissue. Apparently the electrochemistry of neurons requires high metabolic rate. Elaborate metabolic means are used to regulate brain chemistry and to insulate it from the rest of the body which is less sensitive to bad molecules. The blood-brain barrier is the term used to describe this kind of filtering mechanism, which allows only a small number of molecules to enter the nervous system from the blood. It is believed that the glia plays an important role in this function.

1.2. The Classical Neuron

Neurons are cells; they have nucleus and the related metabolic apparatus. Figure 1.1 is a diagram of the generic neuron. In this standard picture, dendrites receive inputs from other cells, the soma and dendrites process and integrate the inputs, and information is then transmitted via the axon to the synapses whose outputs will be inputs to other neurons or to effector organs.

As in all animal cells, the neuron is surrounded by a thin membrane with remarkable properties. Its function is to separate the inside of the neuron from its outside which are chemically very different. The concentration of sodium ions (N_a^+) is as much as 10 times greater outside than inside. Potassium ions (K^+) are equally out of balance, but the concentration is higher inside than outside the cell (for the squid giant axon experiments). Particular ions can pass through the membrane pores (channels) into or out of the cell. The pores can change their conformation under either electrical or chemical control so that ion flow can be regulated; that is, the permeability of the membrane is under the control of the chemical and electrical environment. This mechanism of variable ionic conductance forms the basis for the electric properties of neurons.

Using a patch clamping technique, it is possible to demonstrate and to investigate the properties of single ionic channels. This technique consists of using a hollow glass microelectrode to capture a small piece of a membrane at its tip. This piece actually covers the opening of the microelectrode, and might contain only one or two ionic channels. Then, the ionic and electrical properties of the single channel can be investigated in detail just by studying the minuscule currents passing through it. The channel is seen to open in an on-or-off fashion.

Figure 1.1 shows a generic picture of a neuron in which three main parts can be distinguished. These parts are the soma, the axon and the synapses. The soma, also called the cell body, is the central processing unit element. The hair like processes that emerge from the soma are called dendrites. Besides increasing the surface area for the converging

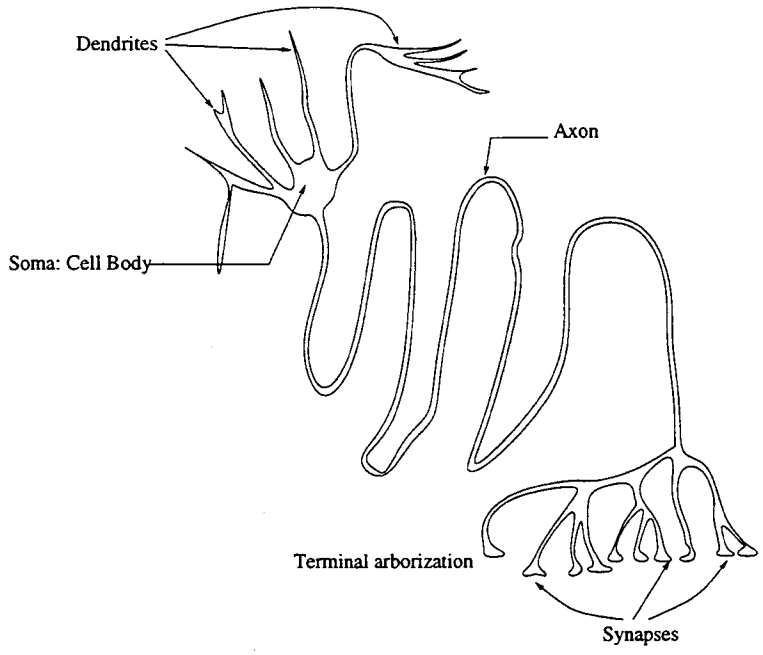

FIGURE 1.1: Generic neuron cell

synapses from other neurons, the role of dendrites in inter-neuron communication is actively under investigation.

The axon is a transmission line of the cell which transports propagated signals from a neuron to another or from a neuron to a muscle tissue. Axons reach their destinations by splitting into several branches referred to as synapses. These terminations broaden into bulges called boutons.

The boutons generally do not make a direct contact with the destination membrane; a cleft, however, separates the two. As shown in figure 1.2, boutons contain small pockets which, under excitation, can release chemicals called neurotransmitters. These chemicals act as mediators in the transfer of activity from the axon to a soma. They modify the permeability of the membrane to different ions in different ways. If the resulting change

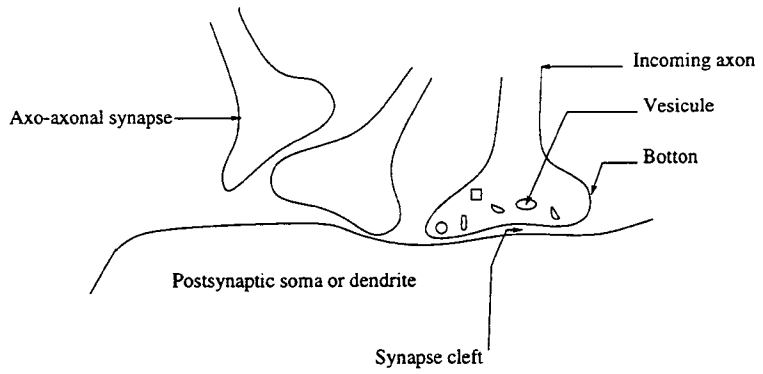

FIGURE 1.2: The synapse

in the potential is positive, it is called an *excitatory postsynaptic potential (EPSP)* and if negative an *inhibitory postsynaptic potential.*

1.3. Neural Electrical Behavior

In order to understand the information abilities of the neurons, one must be able to interpret the electrical events that take place in it. We have mentioned that the neuron has a thin membrane, and that large electrical and chemical differences exist between the inside and the outside of the cell across this membrane.

1.3.1. *The Membrane Potential*

Figure 1.3 shows one of the ways biologists are able to measure the membrane potential. A microelectrode, filled with a conducting solution, is used to measure the potential difference of about $-75\,mV$ across the axon's membrane. Although this potential might appear to be very low, an electric field of about $100,000\,V/cm$ is established across the membrane since it is approximately only $70\,A^o$ thick.

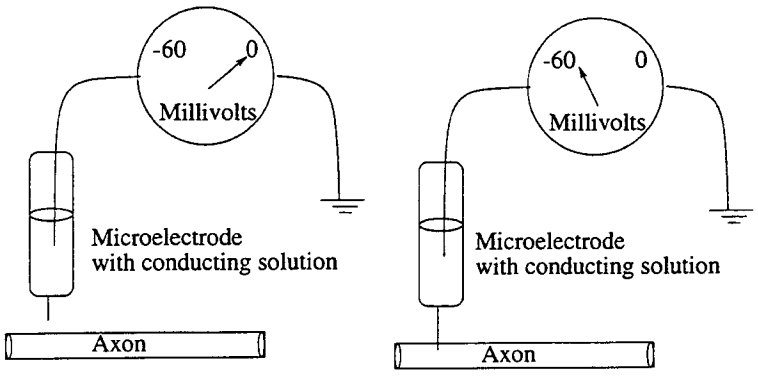

FIGURE 1.3: A microelectrode used to measure the electric properties of a cell.

1.3.2. *Hyperpolarization*

The membrane is said to be hyperpolarized if its voltage is caused to become more negative than the resting potential by a stimulus current that flows across it. As it is illustrated by figure 1.4, the response of a the membrane to a series of hyperpolarizing square current pulses resembles a simple charging and discharging capacitor response.

1.3.3. *Depolarization*

The membrane is said to be depolarized if its voltage is caused to become more positive by a current stimulus. Figure 1.5 shows the response of a depolarized membrane to a square depolarizing current wave[2]. It can be seen that after exceeding a certain level of the input current (threshold), the membrane potential exhibits a special shape called a spike or an action potential. The potential suddenly increases to a maximum value then drops relatively slowly back to its resting equilibrium potential after an undershoot. The action potential shape is different from one type of neurons to another. The mechanism behind the action potential seems to be a regenerative feedback process involving changes

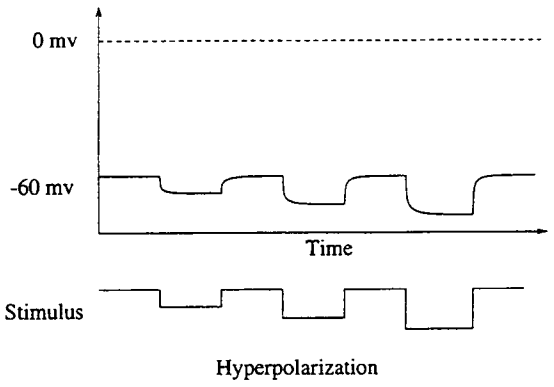

FIGURE 1.4: Electrical response of the neuron to stimulation[2]

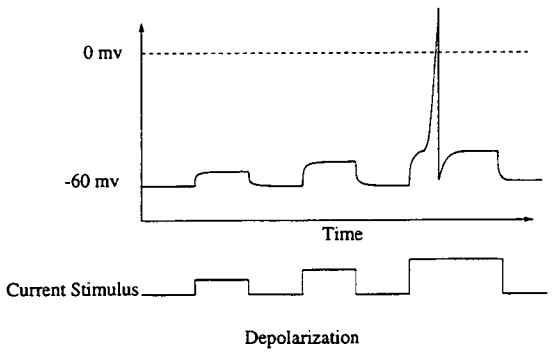

FIGURE 1.5: Electrical response of the neuron to stimulation[2]

in the membrane impedance for particular ions. Hodgkin and Huxley, in their studies on a squid giant axon ([7], [8]), were able to explain many features of the action potential based on the permeability change selectively for sodium and potassium ions. The Hodgkin and Huxley equations provide an elegant mathematical model of the action potential although the physical significance of some variables is not quite clear.

2. SOME MATHEMATICAL MODELS OF NEURONS

2.1. Introduction

In 1902 the physiologist Bernstein[4] stated that the nerve membrane is selectively permeable to potassium ions at rest. Bernstein established that the concentration of K^+ is higher inside the cell than outside and therefore these ions would tend to diffuse out, removing positive charges from the inside of the cell and setting up a negative internal potential. This potential would grow until it is large enough to oppose the further net efflux of K^+ (diffusion and electric forces completely cancel). As it will be seen in the subsequent sections, Nernst's theory[4] is used to calculate the equilibrium potential corresponding to each type of ions.

2.1.1. *Membrane Impedance*

Figure 2.1 shows the property of the membrane impedance change during activity. Cole and Curtis[3] placed an active squid giant axon between two electrodes in an alternating current impedance bridge in order to look for the changes of the membrane resistance and capacitance associated with action potential. They observed a significant fall in the membrane impedance soon after the first sign of depolarization. The decrease in the impedance lasts for some milliseconds after repolarization of the membrane begins.

The time course of the membrane conductance increase in a squid giant axon is measured by the width of the white band photographed from the face of an oscilloscope during the action potential. The band is drawn by the imbalance signal of a high-frequency Wheatstone bridge applied across the axon to measure the membrane impedance[9].

In this work we are interested in how action potentials can be described using system theory and observation of the measurements rather than being too much concerned with cellular anatomy and the details of ionic channels which form the basis of Hodgkin and Huxley models.

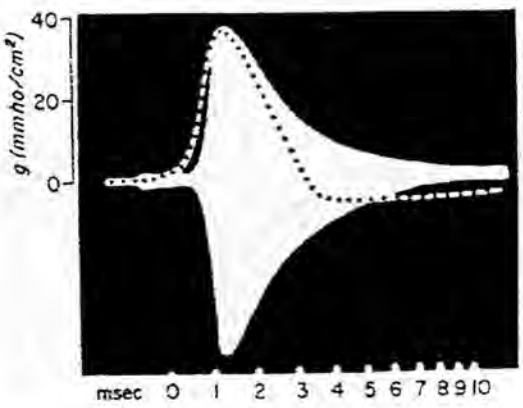

FIGURE 2.1: Membrane conductance increase during propagated action potential. Time course of the action potential is given by the dotted line for comparison. (From Cole & Curtis[3])

Most nerve models are based on Nernst's equation that determines a cell membrane's potential from the ion concentrations near it. This is first discussed in the following section before a brief description of Hodgkin and Huxley model is given.

2.1.2. *Nernst's Equation*

The basis for Nernst's equations is the assumption that ions in a solution act like gas molecules[2]. Therefore, the movement of ions i.e. from inside the cell to outside of it is equivalent to gas expansion from volume V_1 to volume V_2 with ionic concentrations C_1 and C_2 respectively. Under this approximation, Nernst's equation is obtained by equating the work done by ions moving down the concentration difference and the work done by the same ions moving against their electrical gradient[2] and is given by

$$E_{ion} = \frac{kT}{q} \log \frac{C_1}{C_2} \tag{2.1}$$

Equation 2.1 shows how to compute the membrane equilibrium potential, E_{ion}, once the ion concentrations inside and outside are known. q is the charge on each ionized molecule, k the Boltzman constant and T the temperature in degrees Kelvin.

Applying this, independently, to each individual type of the involved ions, particularly sodium (N_a^+) and potassium (K^+) diffusing inwards and outwards respectively, results in an approximation of the corresponding equilibrium potentials given below:

$$E_{N_a} = \frac{kT}{q} \log \frac{C_o^{N_a}}{C_i^{N_a}} = 55mV \tag{2.2}$$

$$E_K = \frac{kT}{q} \log \frac{C_o^K}{C_i^K} = -75mV \tag{2.3}$$

Where $C_{o/i}^{N_a}$ is the sodium concentration outside/inside the cell and $C_{o/i}^K$ is the potassium concentration outside/inside the cell.

2.1.3. *Direct Measurement of Ionic Currents in Axon Membranes*

Hodgkin and Huxley[1] used a voltage clamp method to measure ionic currents associated with different ions in the membrane. Using this method, they developed a kinetic description of the voltage and time dependence of ionic permeability changes in squid giant axon membranes.

2.1.4. *Voltage-Clamp Method*

This method consists of monitoring the voltage across the membrane. Its voltage is kept constant in order to eliminate displacement currents due to the equivalent membrane capacitance which appear in the membrane equation 2.4.

$$I_m = I_i + I_c = I_i + C_m \frac{\partial E}{\partial t} \tag{2.4}$$

As shown by the arrangements depicted in figure 2.2, this is done by means of sensing the difference between the membrane and the reference voltages using a feedback amplifier, then injecting the necessary current to counterbalance ionic currents arising from the change

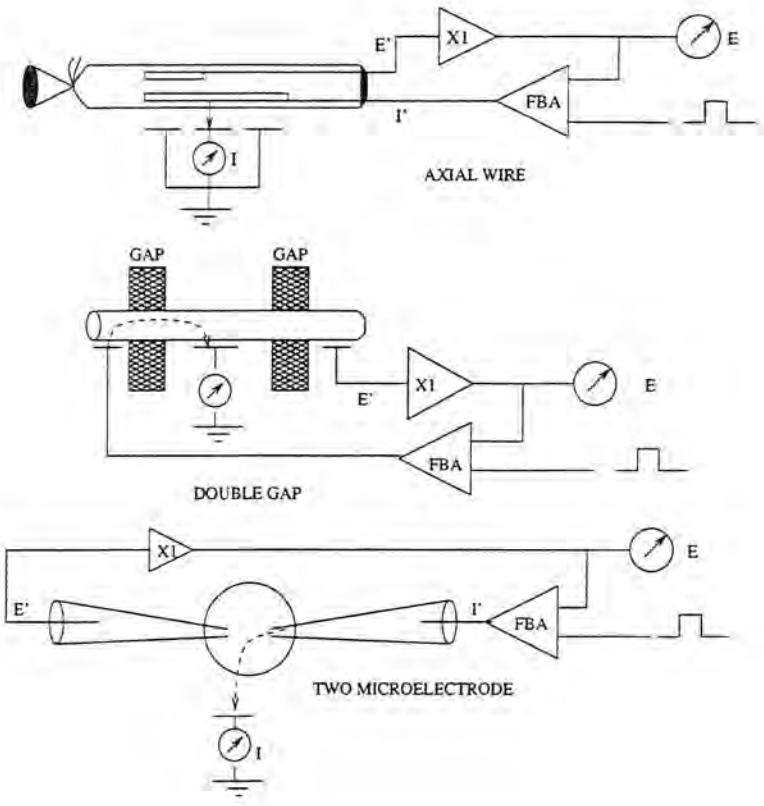

FIGURE 2.2: Three Voltage-clamp methods[4]

in the membrane permeability. The first curve of figure 2.3 shows the total measured current obtained using a hyperpolarizing impulse. The second curve shows that obtained using a depolarizing impulse.

The objective of the method is to calculate the permeabilities to different types of ions from the measured currents. Individual ionic currents must then be known. This is done by using ionic substitution method. By altering the ionic constitution of the bathing solution, Hodgkin and Huxley were able to separate the total membrane current into its main ionic components I_K and I_{Na}.

Curve (A) in figure 2.4 shows the measured current of a portion of a membrane immersed in normal sea water. Curve (B), however, illustrates the ionic current with a

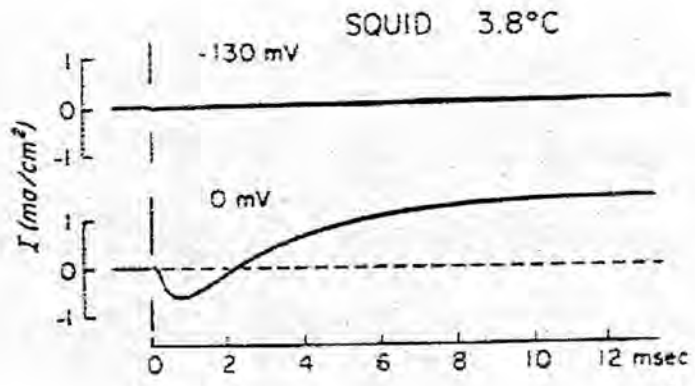

FIGURE 2.3: Recorded voltage-clamp currents with a hyperpolarizing and depolarizing pulses. ([4], ch4, page109).

bathing solution poor in sodium. It, hence, corresponds to a current I_K caused by the movement of potassium ions. The difference between these two curves suggests the course of the component corresponding to the flow of sodium ions.

2.2. Hodgkin and Huxley (HH) Model

Many attempts to describe a nerve cell's electrical behavior have been based on electrical circuit analogies. Hodgkin and Huxley[10] and FitzHugh ([11], [12], [13]) are among those who have taken this approach. The Hodgkin-Huxley model provided a major breakthrough; they formulated a mathematical model that was closely related to experimental data on the squid giant axon membrane.

Using clamping experiments shown in figure 2.2, Hodgkin and Huxley found a simple equivalent electrical circuit, figure 2.5, to model the axon membrane. Their model is instrumental in suggesting and understanding a variety of important experiments, although most neurons are much more complex than squid giant axon.

In figure 2.5, the membrane current consists mainly of the portion which charges the membrane capacitance and a portion associated to the ionic currents. Ionic currents are

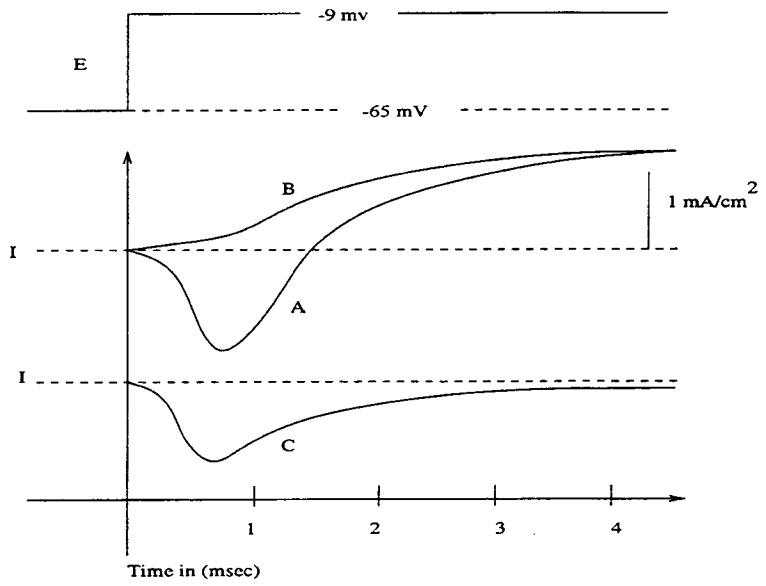

FIGURE 2.4: Separation of ionic currents in squid giant axon by ionic substitution method. ([4], ch4, page110).

subdivided into three distinct components, a sodium current I_{Na}, a potassium current I_K and a small leakage current I_L which is primarily carried by chloride ions. Equation 2.5 describes the behavior of the circuit shown in figure 2.5.

$$C_m \frac{dV_m}{dt} + I_{ion} = I_{ext} + I_{synapse} \tag{2.5}$$

Here C_m is the membrane capacitance, V_m is the intracellular potential (membrane potential), I_{ion} is the net ionic current flowing across the membrane, I_{ext} is an externally applied current, $I_{synapse}$ is the synaptic current fed by neighboring cells. Synaptic current is ignored in the model of a single neuron.

2.2.1. *Hodgkin and Huxley Conventions*

In equation 2.5 I_{ion} and I_{ext} have opposite sign conventions[14]. As this equation is written, positive I_{ext} will tend to depolarize the cell (i.e., V_m more positive), while negative

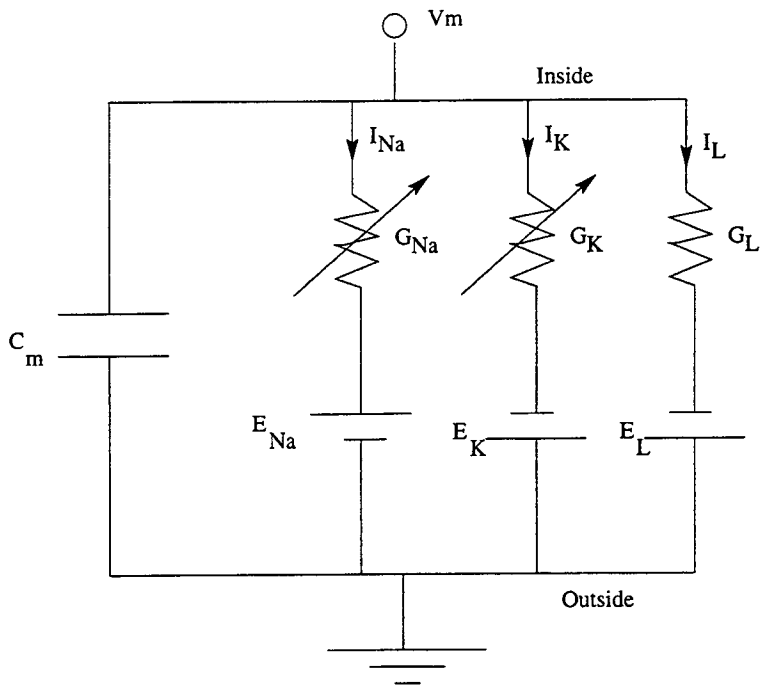

FIGURE 2.5: Hodgkin and Huxley model equivalent circuit.

I_{ext} will hyperpolarize it (i.e., make V_m more negative). This sign convention is sometimes referred to as the *physiologists convention* which states that an inward flow of positive ions into the cell is considered a negative current[14].

2.2.2. *Ionic Currents*

The total ionic current is the algebraic sum of the individual contributions from all participating ion types.

$$I_{ion} = \sum_k G_k(V_m - E_k). \tag{2.6}$$

Where G_k is the conductance, the inverse resistance $G_k = 1/R_k$, associated with component

ionic component I_k. As described above, in HH-model there are 3 types of these ionic components, hence;

$$I_{ion} = G_{Na}(V_m - E_{Na}) + G_K(V_m - E_K) + G_L(V_m - E_L). \tag{2.7}$$

In order to explain their experimental results, Hodgkin and Huxley postulated that G_{Na} and G_K both change dynamically with the membrane voltage. It is proven today that this voltage dependence can be related to the biophysical properties of the membrane that control the flow of ions across the membrane.

Today, it is scientifically believed that the cell membrane contains ion-selective paths which are called channels. These regulate the flow of ions through the membrane by closing or opening depending on the value of the membrane potential.

Although Hodgkin and Huxley did not know much about these channels at the time they developed their model; the validity of their assumptions and the results of many modern experiments enable us to describe their model in terms of these ionic channels.

> The macroscopic conductance G_k of the HH model can be thought of as arising from the combined effects of a large number of microscopic ion channels embedded in the membrane. Each individual ion channel can be thought of as containing a small number of physical *gates* which regulate the flow of ions through the channel. An individual gate can be in one of two states, permissive or non-permissive. When all of the gates of a particular channel are in the permissive state, ions can pass through the channel and the channel is open. If any of the gates are in the non-permissive state, ions cannot flow and the channel is closed ([14], page:37).

In HH- model, the ionic conductances are assumed to be functions of the membrane voltage by stating that the probability for an individual gate to be in the permissive or non-permissive state depends on the membrane voltage. i.e. for a specific gate i the associated probability to be in the permissive state, is P_i which ranges from 0 to 1. Large number of gates rather than an individual one could be taken into account using the fraction of

gates in that population that are in the permissive state and $(1 - p_i)$ as the fraction in the non-permissive state. Hodgkin and Huxley assumed that transitions between permissive and nonpermissive states obey first order kinetics:

$$\frac{dp_i}{dt} = \alpha_i(V)(1 - p_i) - \beta_i(V)p_i \tag{2.8}$$

Where α_i and β_i are voltage-dependent rate constants describing the "non-permissive to permissive" and "permissive to non-permissive" transition rates, respectively[14]. If the membrane is clamped to a certain value V, then the fraction of gates in the permissive state will eventually tend to a steady state value with $dp_i/dt = 0$ as t tends to ∞:

$$p_{i,t\to\infty}(V) = \frac{\alpha_i(V)}{\alpha_i(V) + \beta_i(V)}. \tag{2.9}$$

The time constant of the exponential representing the time course for approaching this equilibrium point is given by

$$\tau_i(V) = \frac{1}{\alpha_i(V) + \beta_i(V)}. \tag{2.10}$$

An individual channel is considered open when all the gates in that channel are open. When a channel is open, it contributes with a small fixed percentage to the total conductance and zero otherwise. The macroscopic conductance associated with a large population of channels is proportional to the number of channels in open state, and hence to the probability that the associated gates in their permissive state. Therefore it is just fear to say that the macroscopic conductance G_k due to channels of type k, with constituent gates of type i, is proportional to the product of the individual gate probabilities p_i:

$$G_k = \bar{g}_k \prod_i p_i \tag{2.11}$$

In equation 2.11, $\bar{g}_k$ is a normalized constant which represents the maximum conductance when all the channels are open.

The variable p_i in equations 2.8– 2.11 is the generalized notation that could be applied to a variety of conductances. In the HH-model, this variable is replaced by other variables which take the names of the associated gate types. For instance, the HH-model models the

sodium conductance using three gates of type labeled "m" and one gate of type labeled "h". Hence,

$$G_{Na} = \bar{g}_{Na} p_m^3 p_h \equiv g_{Na} m^3 h \tag{2.12}$$

Similarly, the potassium conductance is modeled with 4 gates of the same type "n"

$$G_K = \bar{g}_K p_n^4 \equiv \bar{g}_K m^4 \tag{2.13}$$

2.2.3. *HH-model Equations*

The following is the summary of the HH-model equations:

$$I_{ion} = \bar{g}_{Na} m^3 h (V_m - E_{Na}) + \bar{g}_K n^4 (V_m - E_K) + \bar{g}_L (V_m - E_L) \tag{2.14}$$

$$\frac{dm}{dt} = \alpha_m(V_m)(1-m) - \beta_m(V_m)m, \tag{2.15}$$

$$\frac{dh}{dt} = \alpha_h(V_m)(1-h) - \beta_h(V_m)h, \tag{2.16}$$

$$\frac{dn}{dt} = \alpha_n(V_m)(1-n) - \beta_n(V_m)n, \tag{2.17}$$

The experimentally observed values of α's and β's are represented approximately by smooth mathematical functions. The functions for squid axons at 6.3°C are

$$\alpha_m = \frac{0.1(V_m + 40)}{1 - e^{-(V_m+40)/10}} \tag{2.18}$$

$$\beta_m = 0.108 e^{-V_m/18} \tag{2.19}$$

$$\alpha_n = \frac{0.01(V_m + 55)}{1 - e^{-(V_m+55)/10}} \tag{2.20}$$

$$\beta_n = 0.0555 e^{-V_m/80} \tag{2.21}$$

$$\alpha_h = 0.0027 e^{-V_m/20} \tag{2.22}$$

$$\beta_h = \frac{1}{1 + e^{-(V_m+35)/10}} \tag{2.23}$$

The constant parameters which appear in equation 2.14, used in simulating the HH-model in this research, are[4] $E_{Na} = 50\,mV$; $\bar{g}_{Na} = 120\,mmho/cm^2$; $E_k = -77\,mV$; $\bar{g}_k = 36\,mmho/cm^2$ $E_L = -54.387\,mV$; $\bar{g}_L = 0.3\,mmho/cm^2$; $C_m = 1\mu F/cm^2$.

3. A SIMPLE BANG-BANG CONTROLLED BILINEAR MODEL

3.1. Introduction

Most of the physical behavior of the squid giant axon seems to be adequately approximated by the Hodgkin and Huxley (HH) model ([1], [8], [10], [15]). This model basically represents an electrical equivalent circuit of a neuron membrane. The equivalent circuit takes into account the membrane capacitance, the membrane voltage dependent potassium and sodium conductances with their respective equilibrium voltages. In addition, a leakage branch is included to account for other types of ions involved. Figure 3.1 shows the action potential and the gate parameters which result from simulating HH-model equations 2.14-2.23. Of particular interest in this work is the membrane voltage graph which shows an action potential. The aim is to reproduce the shape of this spike using bang-bang switching between two second-order systems. Figure 3.2, on the other hand, shows the variable sodium and potassium conductances over the spike duration. These are obtained from simulations of equations 2.12 and 2.13 respectively.

It can be seen that the HH-model, depicted by figure 2.5, is a variable-structure impedance model. The impedance that the membrane presents to the flow of ions changes depending on the voltage across it. This structure change can be approximated by a piecewise linear structure called a bang-bang feedback control or a bilinear system (BLS) with constant piecewise constant coefficients.

In the HH-model, the sodium and potassium conductances are continuously controlled by the corresponding ionic feedback. However, the feedback ion-gate model components are quite complex and not physically satisfying, but mostly generated to fit the data. The present work intends to generate a simple and somewhat physically meaningful model based on a variable-structure impedance to sodium and to potassium ion currents. Hence, basic system theory is used to simulate the apparent features of two jointly-linked linear structures to form a bang-bang controlled bilinear system. These features are obvious when observing the membrane potential spike after it is excited with a current impulse.

In this chapter, the membrane spike-signal shape is first approximated using switching between two second-order systems. One of which exhibits a stable focus as an equilibrium point and the other a saddle point. Then, introducing a third linear system, with a stable focus equilibrium point, will improve the approximation of the spike shape.

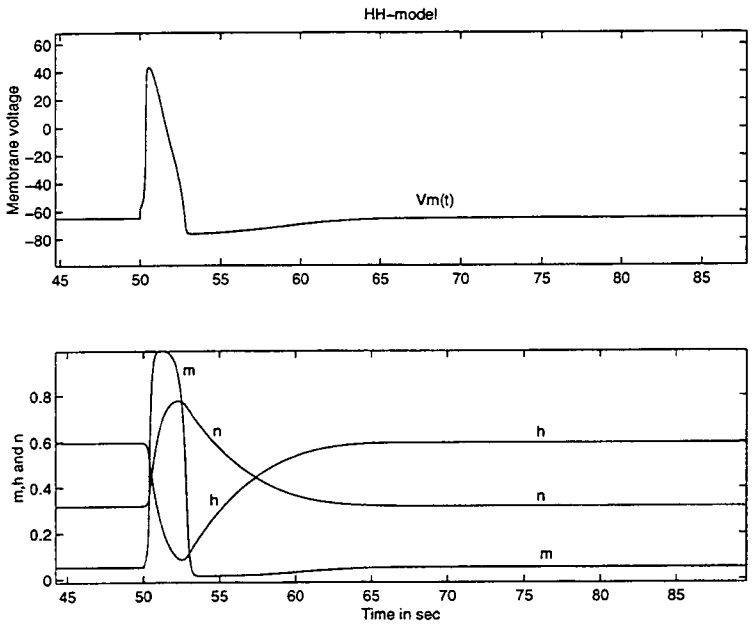

FIGURE 3.1: Voltage spike and m, h and n variations during the excitation of HH model with a short current impulse.

By observing the response of a neuron to an EPSC (excitatory postsynaptic current), we can easily deduce that the spike acts as if produced first by a second-order system with a saddle point which switches to another second-order system with a stable focus equilibrium point with a relatively high damping ratio and appropriate natural frequency. In this chapter, we will show how the model helps approximately reproduce a spike shape

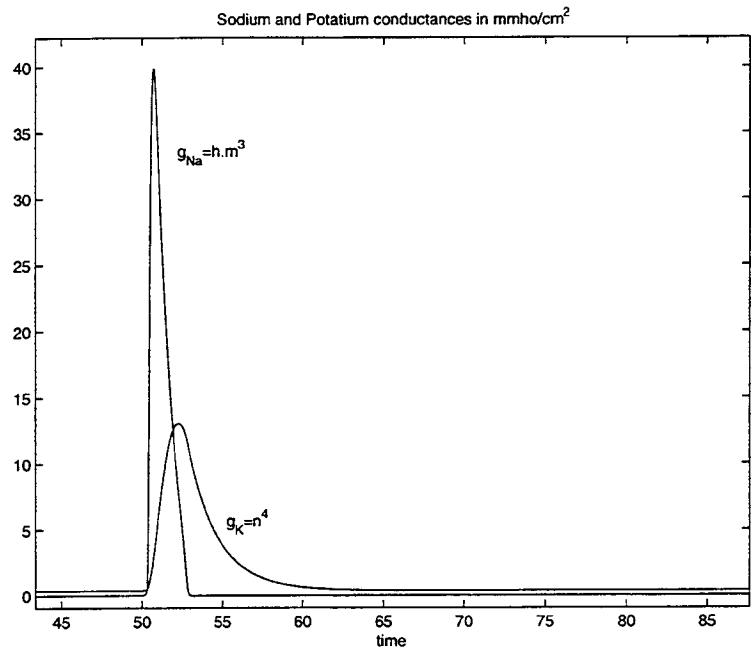

FIGURE 3.2: Sodium and Potassium conductances—HH model— versus time during the spiking.

similar to the experimentally observed one.

3.2. Background on Second Order Systems

Assume we have the following two linear differential equations:

$$\ddot{v} + a_1\dot{v} + b_1 v = 0 \tag{3.1}$$

$$\ddot{v} + a_2\dot{v} + b_2 v = 0 \tag{3.2}$$

The system described by the differential equation 3.1 is to have a saddle point at the membrane voltage inflection, where the voltage starts to shoot up. Whereas the system

described by the second differential equation 3.2, is to have a stable focus at the equilibrium potential, since after firing, the potential falls back to settle around the rest potential after a small undershoot.

3.2.1. *Stable Focus*

For the system described by equation 3.1 to have a stable focus, its characteristic polynomial $S^2 + a_1 S + b_1 = 0$ should have 2 complex conjugate roots with a negative real part. The two roots are given by the following,

$$S_{1,2} = \frac{-a_1 \pm \sqrt{a_1^2 - 4b_1}}{2} \tag{3.3}$$

The conditions for the stable focus equilibrium point are then,

$$a_1 > 0 \tag{3.4}$$

$$a_1^2 - 4b_1 < 0 \tag{3.5}$$

The region for the selection of a and b to satisfy these two conditions is shown by the shaded area in figure 3.3

3.2.2. *Saddle Point*

For the system to have a saddle point, the characteristic equation should have two distinct-in-sign real roots. The condition for this to occur is that the product of S_1 and S_2 given by equation 3.3 is negative. Hence b is negative as shown by figure 3.3.

In the state space representation of this system, notice that the eigenvalues are just the slopes of the two lines representing the eigenvectors for $\dot{v}$ vs v. This is shown in the following.

If we let $x_1 = v$ and $x_2 = \dot{x}_1$ then

$$\dot{x}_1 = x_2 \tag{3.6}$$

$$\dot{x}_2 = -ax_2 - bx_1 \tag{3.7}$$

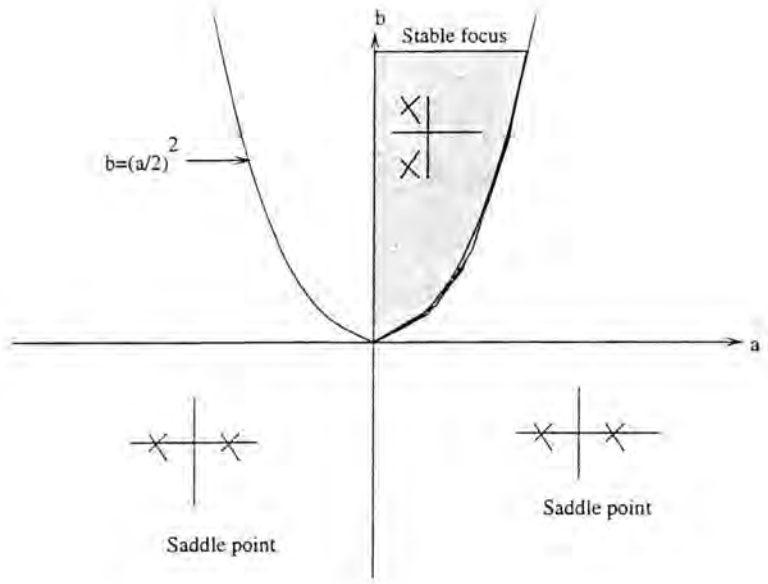

FIGURE 3.3: a and b regions for stable node and saddle point.

Which, with $X = \begin{pmatrix} x_1 \\ x_2 \end{pmatrix}$, can be written as $\dot{X} = \begin{pmatrix} 0 & 1 \\ -b & -a \end{pmatrix} X$

If $V_1 = \begin{pmatrix} v_{11} \\ v_{12} \end{pmatrix}$ and $V_2 = \begin{pmatrix} v_{21} \\ v_{22} \end{pmatrix}$ are two eigenvectors corresponding to S_1 and S_2 respectively, then, their components are related as in the following relationships,

$$v_{12} = S_1 v_{11} \tag{3.8}$$

$$v_{22} = S_2 v_{21} \tag{3.9}$$

Hence one can change the values of the eigenvalues to adjust how fast the spike will shoot up towards the switching point. As to the stable-focus system, both the natural frequency and the damping ratio are altered to achieve the desired overshoot.

Figure 3.4 shows an example of state space solution of a system obtained by switching from a saddle point at point $(0, 0)$ to a stable focus at $(-0.5, 0)$. The switching occurs

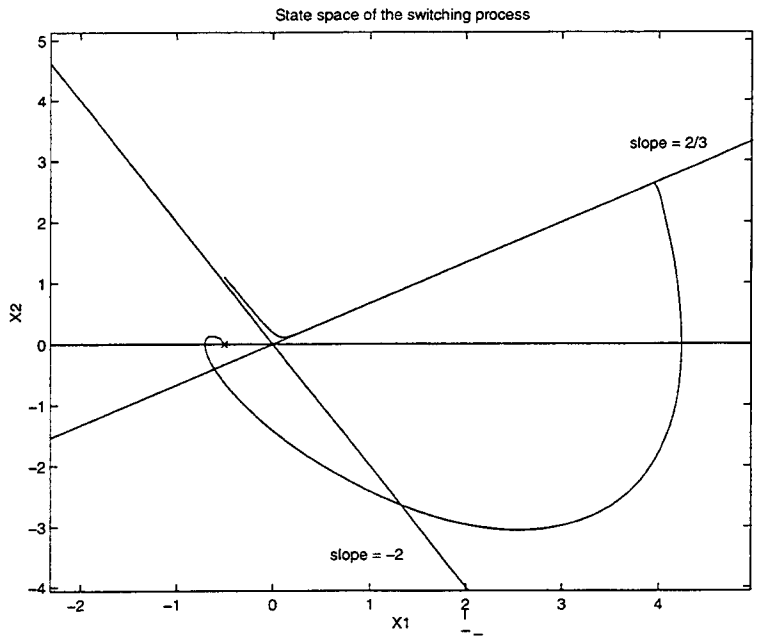

FIGURE 3.4: State space representation of the switching process

at a predetermined value of the membrane potential representing the sodium equilibrium voltage V_{Na}. The system obtained from combining both equations 3.1 and 3.2 forms a bilinear system[16].

$$\ddot{x} + \frac{5}{12}\dot{x} - \frac{11}{12}x + \frac{1}{3} - u\left(\frac{11}{12}\dot{x} - \frac{5}{12}x + \frac{1}{3}\right) = 0 \tag{3.10}$$

with bang-bang control

$$u = \begin{cases} -1 & \text{if } \dot{x} > S_1 x \text{ and } \dot{x} > S_2 x \text{ and } x \leq V_{Na} \\ +1 & \text{else} \end{cases} \tag{3.11}$$

These are obtained using $\zeta = 0.707$ and $\omega_n = \sqrt{(2)}$ for the stable focus ($a_1 = -0.5$, $b_1 = -0.5$) and $S_1 = -2$ and $S_2 = 2/3$ for the saddle point ($a_2 = 4/3$, $b_2 = -4/3$).

Figure 3.5 shows that the bilinear system can explain the shape of the neuron spike, although different neurons of different species exhibit different spike shapes, important

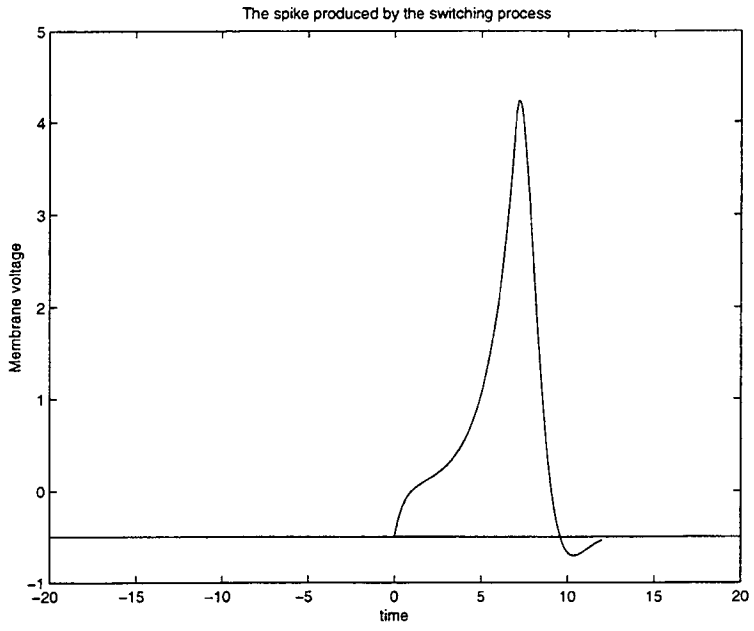

FIGURE 3.5: Spike obtained from the bilinear system

features of the membrane could be approximated by the appropriate piecewise linear characteristics corresponding to the bang-bang controlled membrane impedance. This is the subject of the subsequent chapters.

Figure 3.5 stresses the similarity between the HH-spike and that generated using a bilinear model. Although the initial inflection is not quite apparent in figure 3.1, neurons do exhibit this behavior when the excitation is just strong enough to produce an action potential. Depending on the strength of the current impulse input, the action potential rises rapidly or through a significant initial inflection point. In the BLS-model, this could be accounted for by altering the firing threshold above the negative switching eigen vector line.

Here, the permeability of the membrane to sodium ions is represented by the unstable equilibrium point part (saddle). The period during which the potential rises—along the positive eigen vector—could be thought of as the flow of sodium ions from the outside of

the membrane to the inside, just as described by Hodgkin and Huxley. This situation does not last long before the permeability of the membrane to potassium ions takes over, and the membrane potential drops back to approach its equilibrium potential. This is represented by the stable focus portion of figure 3.5.

3.3. Neuron Properties

The desired model simplification of a single neuron is compared to the HH-model in light of some properities which neurons exhibit. It is therefore worthwile mentioning some of these characteristics before any further analysis.

3.3.1. *Pulse Timing*

Communication between neurons has been approached from different perspectives. Some models assume instantaneous activated synapses by graded potential changes between neurons. Others assume discontinuous communication which takes place via synapses activated by propagated action potentials (spikes).

In the latter category, relative presentation of stimulating current impulses (or action potentials) are found to have interesting effects on the timing of the neuron's membrane firing[5]. The relationship of the spike appearance time to the strength and the presentation time of afferent impulses is given by curves referred to as input and output curves (I/O-curves).

3.3.2. *I/O properties of single Neurons*

As it is shown in figure 3.6, the model consists of two distinct neurons[1]. The neurons are normally at rest. Cell-1 is used to provide an EPSP signal just strong enough to cause cell-2 to spike. Depolarizing (DI) and hyperpolarizing impulses are used to model the effect of converging influences of different magnitudes from the neighboring cells. DH's and DI's are very short (one integration step) and the voltage changes they produce is well within the linear region of the membrane. Figure 3.7 shows three superposed simulations' independent

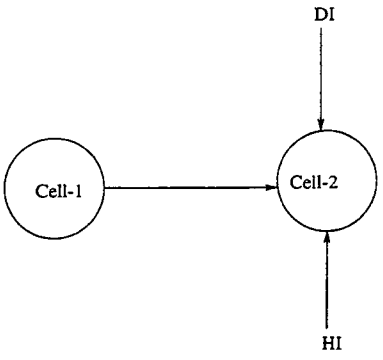

FIGURE 3.6: Perturbation of a neuron cell by hyperpolarizing and depolarizing impulses[5]

sweeps. The dashed curve shown in panel (A) is the unperturbed spike, with the application of the EPSC (B) only. The dotted and continuous curves represent the evoked spikes with the application of DI and HI perturbing impulses respectively. It is clear that depolarizing impulses advance the spiking event while hyperpolarizing impulses delay it.

The time it takes for the action potential (spike) to reach the threshold voltage, with respect to some given reference (in this case it is the beginning of each sweep), is recorded and plotted against the presentation time of the corresponding impulses. Different curves for different perturbing impulse amplitudes are obtained and the their collection is called *I/O-functions* or *Latency curves*(referred to as Input-Output, I/O, functions for the experiment). Their shapes are shown in figure 3.8.

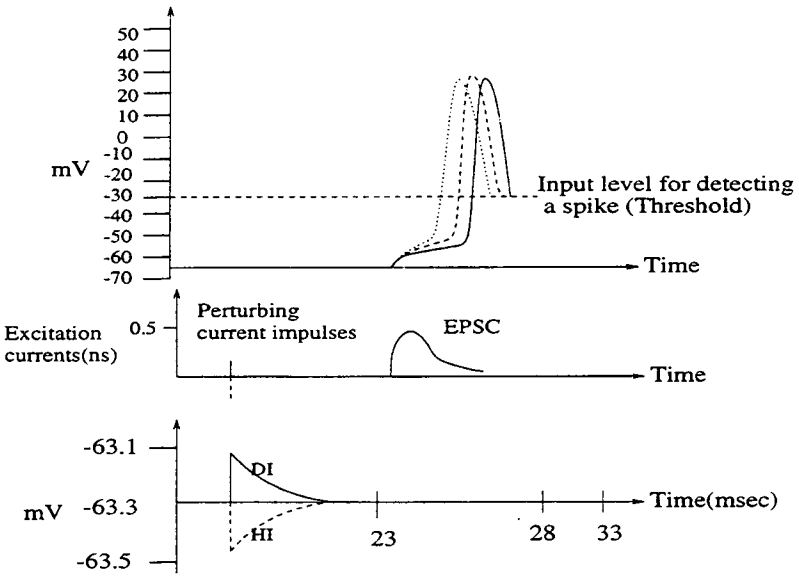

FIGURE 3.7: Three superimposed simulation sweeps[5]

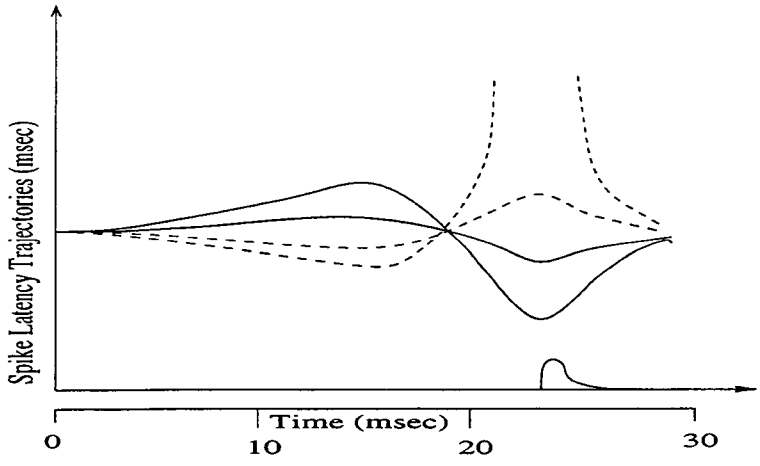

FIGURE 3.8: Latency (I/O) curve shapes[5]

3.4. Inductance Effect in the Ionic Channel

3.4.1. *Inductive feature of a neuron membrane*

A significant evidence of an equivalent inductive effect in the membrane of a neuron cell was illucidated by some HH-model simulation results consisting of calculating the average voltage to current ratio across the membrane. Figure 3.9 shows three impedance plots obtained under different conditions; normal resting, depolarized, and hyperpolarized membrane[5].

The impedance curves shown in figure 3.9 are obtained from simulations on the Hodgkin-Huxley (HH) neuron model. They portray the fact that depolarizing the membrane enhances the appearance of the inductive effect. Since during depolarization the membrane becomes much more permeable to sodium ions, this suggests that particularly sodium paths should be modeled to include inductance (lead in phase) as opposed to potassium paths which show much less inductive effect when their ions are favored by the membrane permeability.

Although appropriate experimental data has not been available to this project, we use the data from HH-model simulations as this is broadly accepted for the squid giant axon.

3.4.2. *General Model of an Ionic Channel*

Simulated HH-model data, such as figure 3.9 suggest that the actual network shown in figure 3.10 should include some inductance. Here,

$$i_{ex} = i_c + i_{ch} \tag{3.12}$$

$$i_c = C_m \frac{dv_m}{dt} \tag{3.13}$$

$$(v_m + E_{ch}) = R_{ch} i_{ch} + L_c \frac{di_{ch}}{dt} = R_{ch}(i_{ex} - i_c) + L_{ch} \frac{di_{ch}}{dt} \tag{3.14}$$

From equation 3.12, we have

$$\frac{di_{ex}}{dt} = C_m \frac{d^2 v_m}{dt^2} + \frac{di_{ch}}{dt} \tag{3.15}$$

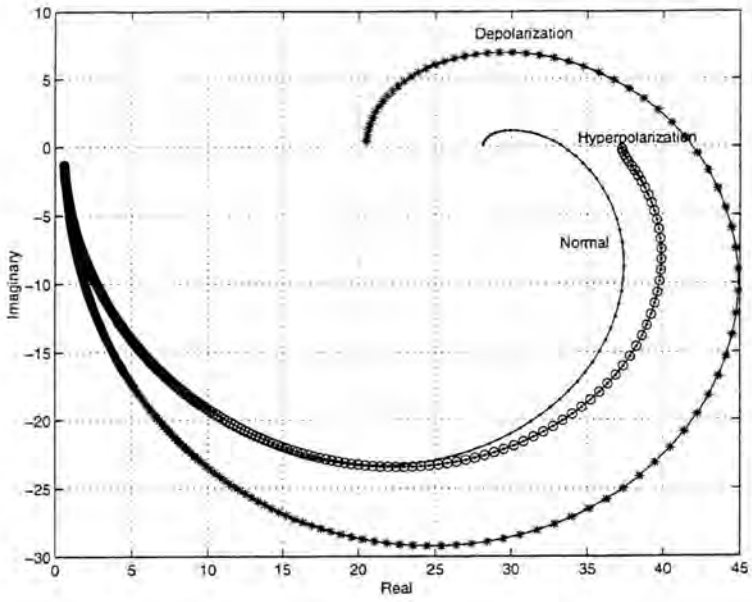

FIGURE 3.9: Impedance plots of a neuron membrane under subthreshold conditions. They are obtained by simulations of HH-model[5]

Using equation 3.14, we get

$$\frac{di_{ex}}{dt} = C_m \frac{d^2 v_m}{dt^2} + \frac{1}{L_{ch}} \left[(v_m + E_{ch}) - R_{ch}(i_{ex} - C_m \frac{dv_m}{dt}) \right] \tag{3.16}$$

Rearranging the equation above, we obtain the following equation, in which a lead term originating from the existence of the channel inductance appears.

$$C_m \frac{d^2 v_m}{dt^2} + \frac{C_m R_c h}{L_{ch}} \frac{dv_m}{dt} + \frac{1}{L_{ch}} (v_m + E_{ch}) = \frac{di_{ex}}{dt} + \frac{R_{ch}}{L_{ch}} i_{ex} \tag{3.17}$$

Or

$$\frac{d^2 v_m}{dt^2} + \frac{R_{ch}}{L_{ch}} \frac{dv_m}{dt} + \frac{1}{L_{ch} C_m} (v_m + E_{ch}) = \frac{1}{C_m} \frac{di_{ex}}{dt} + \frac{R_{ch}}{L_{ch} C_m} i_{ex} \tag{3.18}$$

Which could be written as a transfer function from i_{ex} to v_m as:

$$\frac{V_m(s)}{I_{ex}(s)} = K \frac{\omega_n^2 (s + \alpha)}{s^2 + 2\zeta\omega_n s + \omega_n^2} \tag{3.19}$$

where, $K = L_{ch}$, $\omega_n = 1/\sqrt{L_{ch} C_m}$, $\alpha = R_{ch}/L_{ch}$, $\zeta = R_{ch}\sqrt{C_m/L_{ch}}$.

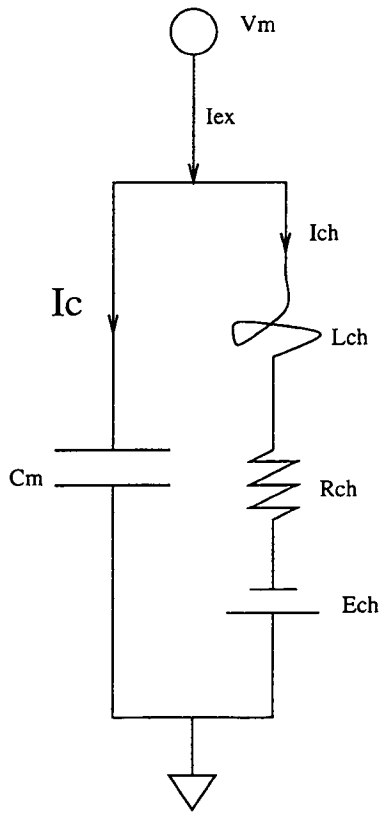

FIGURE 3.10: Equivalent circuit of a membrane channel.

The time domain impulse response, V_{mir}, of the system represented by equation 3.19 is given by the following equation:

$$V_{mir}(t) = \omega_n \sqrt{\frac{\alpha^2 - 2\alpha\zeta\omega_n}{1-\zeta^2}} e^{-\zeta\omega_n t} \sin\left(\omega_n\sqrt{1-\zeta^2}t + \theta\right) \tag{3.20}$$

where

$$\theta = tan^{-1}\frac{\omega_n\sqrt{1-\zeta^2}}{\alpha - \zeta\omega_n} \quad (\zeta < 1) \tag{3.21}$$

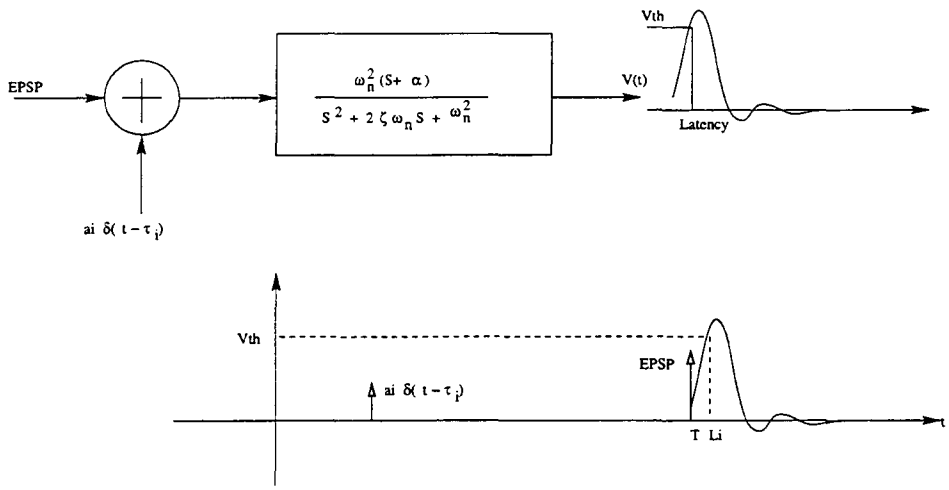

FIGURE 3.11: Latency simulations

3.4.3. *Latency Experiments on a Simple Second-Order System*

Figure 3.11 shows a block diagram of a second-order system as used in chapter 4. with the added lead term suggested above. It also shows how the latency is measured. A strong primary input impulse is presented at a fixed point in time. Secondary perturbing impulses are presented at different time positions prior to the the primary one. For each amplitude A_i of the perturbing impulses, their presentation time is varied to sweep the entire time interval prior to the primary input impulse. Latency curves are obtained by plotting the time, L_i, at which the output voltage reaches V_{th} against these presentation times, for different values of A_i. Initial time of each simulation is taken to be the time origin. Appendix B provides the required parameters for the implementation of the same simulation using simulink system blocks. It also provides the driving matlab program, written to vary the presentation time and record the latency.

The values used in this experiment are $\zeta = 1/\sqrt{2}$, $\omega_n = \sqrt{2}$, similar to the stable focus mode in section 3., but with $\alpha = 5$.

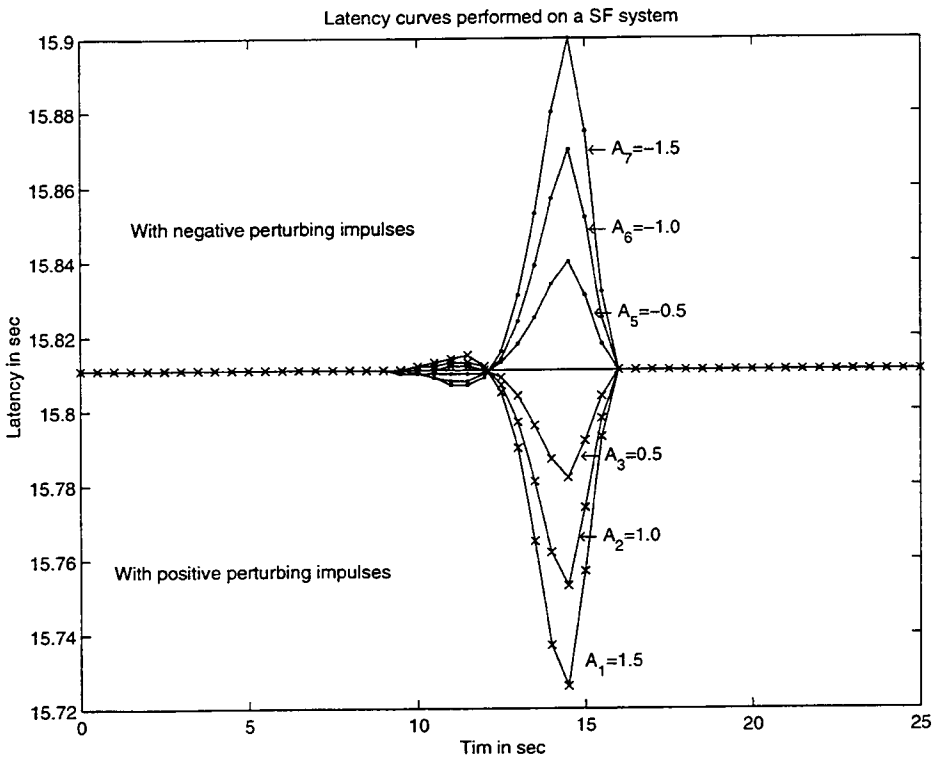

FIGURE 3.12: Depolarization and Hyperpolarization latency curves. A_i are the amplitudes of the perturbing impulses.

Figure 3.12 shows the obtained latency time trajectories (see chapter 3), corresponding to positive perturbing impulses (Depolarization) and others corresponding to negative impulses (hyperpolarization) for this simple model.

These curves show a natural feature of this linear system class. They are closely related to the published latency curves obtained from the Hodgkin and Huxley model with similar experiments as shown in figure 3.8.

However, note a slight lack of symmetry in figure 3.8 (not present in figure 3.12) probably due to the change in the model parameters according to impulse sign and magnitude, through the nonlinear feedback in the HH-model.

4. SINGLE NEURON MODEL

4.1. Introduction

In this section, a preliminary study of a basic switching problem, which is based on section 3.1. is presented. In this part of work, only one type of input, delta-functions form change in current, $A\sum\delta(t-t_i)$ is considered. The switching threshold for going from one mode to another will be determined according to both the voltage and its rate of change levels as appropriate for a second-order system. Again, the switchings correspond to discrete impedance changes as for potassium and sodium ions.

4.2. Refractoriness

In order to account for the fact that the membrane is totally insensitive to the incoming impulses, received while spiking and before the membrane voltage settles within a particular range around the SF equilibrium point, a third nonlinearity (relay) is used to disable the excitation after the first switching and enable it again after the voltage signal enters a zone defined by a circle of radius ϵ centered around the stable focus equilibrium point. Although it appears, from simulations performed on the HH-model, that the membrane restores its sensitivity to input pulses in a progressive manner, an ideal relay is used here for illustration purposes. In the following paragraphs, a procedure is developed to determine the logic needed.

4.3. Threshold Determination

As mentioned in the introduction, Dirac type impulses are considered primarily as the inputs for the model. During the initial phase, the membrane is at rest. The resting potential is assumed zero in this analysis. A current impulse is applied to the membrane and depending on the area of this impulse, the membrane may or may not fire. Let both coefficients of the left hand side of equation 3.18 be equal to 2, (damping coefficient of 0.707

and the natural frequency of $\sqrt{2}$[1], and let A be the coefficient of the applied Dirac impulse.

$$\frac{d^2v_m}{dt^2} + 2\frac{dv_m}{dt} + 2v_m = A\delta(t) \tag{4.1}$$

The solution for equation 4.1 is given by the following,

$$v_m(t) = Ae^{-t}\sin(t) \tag{4.2}$$

with the initial conditions $v_m(0) = 0$ and

$$\left.\frac{dv_m}{dt}\right|_{t=0} = A\left[-e^{-t}\sin(t) + e^{-t}\cos(t)\right]_{t=0} = A \tag{4.3}$$

If the equilibrium point corresponding to the saddle point is V_{sp}, and if λ_1 is the negative eigenvalue corresponding to the saddle point, then the condition for firing is given by:

$$A = \dot{v}_m|_{t=0} \geq -\lambda_1 V_{sp} \tag{4.4}$$

In general, the spiking threshold at $v_m = x$ is set to be

$$A = \dot{V}_{mth} = \lambda_1(x - V_{sp}) \tag{4.5}$$

when saddle equilibrium point, V_{sp}, is not at the origin.

Figure 4.1 shows the switching operations by means of comparators and other logic. Figure 4.2 gives the phase plot of the two states of the model.

The relay shown in figure 4.1 is used to implement the refractory property. As mentioned in section 4.2., the circles included in figure 4.2 account for the refractoriness. By means of a relay, the input is disabled as soon as the firing threshold is reached and is enabled again when the trajectory enters a recovery zone defined by a circle of radius ϵ in the phase plot, within which the neuron is assumed to have completely restored its sensitivity to the input signal. This is taken to be $Vth/50$ in preliminary simulations. The spiking threshold sets the relay's higher switching point while the recovery region sets its lower switching limit.

[1]These values are normalized to rad/msec in order to approximate the neuron response.

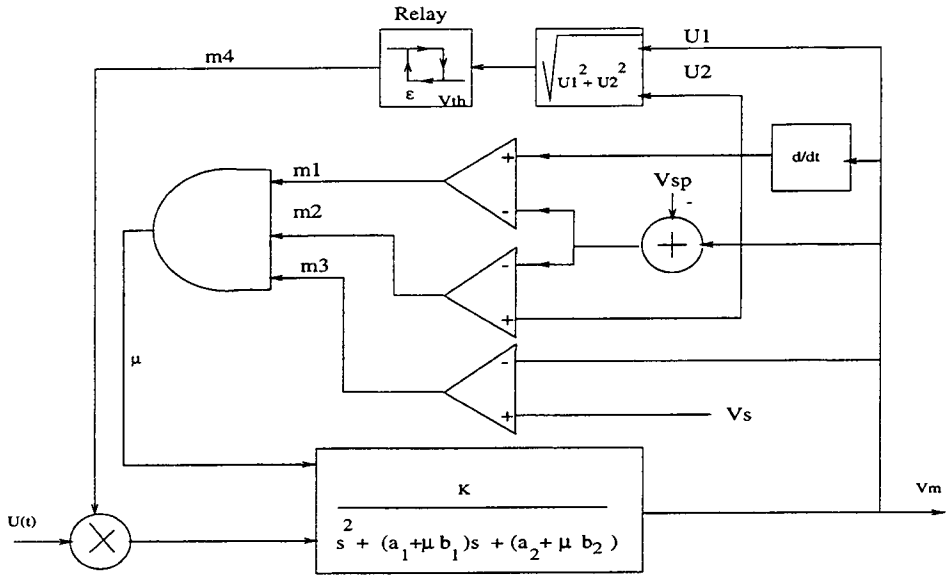

FIGURE 4.1: Block diagram of the Switching circuit

The general equation of the system described by figures 4.1 and 4.2 could be written as follows.

$$
\begin{cases}
\ddot{v}_m + (a_1 + ub_1)\dot{v}_m + (a_2 + ub2)v = m_3 A\delta(t) \\
u = m_1 \cdot m_2 \cdot m_3 \\
m_1 = \begin{cases} 1 & \dot{v}_m \geq \lambda_1(v_m - V_{sp}) \\ 0 & \text{elsewhere.} \end{cases} \\
m_2 = \begin{cases} 1 & v_m > \lambda_2(v_m - V_sp) \\ 0 & \text{elsewhere} \end{cases} \\
m_3 = \begin{cases} 1 & v_m \leq V_s \\ 0 & \text{elsewhere} \end{cases} \\
m_4 = \begin{cases} 1 & \zeta(t) = \sqrt{{v_m}^2 + \dot{v}_m^2} \leq \epsilon \quad \text{and} \quad m_{4\_} = 0 \\ 0 & \zeta(t) \geq \dot{v}_{mth}(t) \quad \text{and} \quad m_{4\_} = 1 \end{cases}
\end{cases}
\tag{4.6}
$$

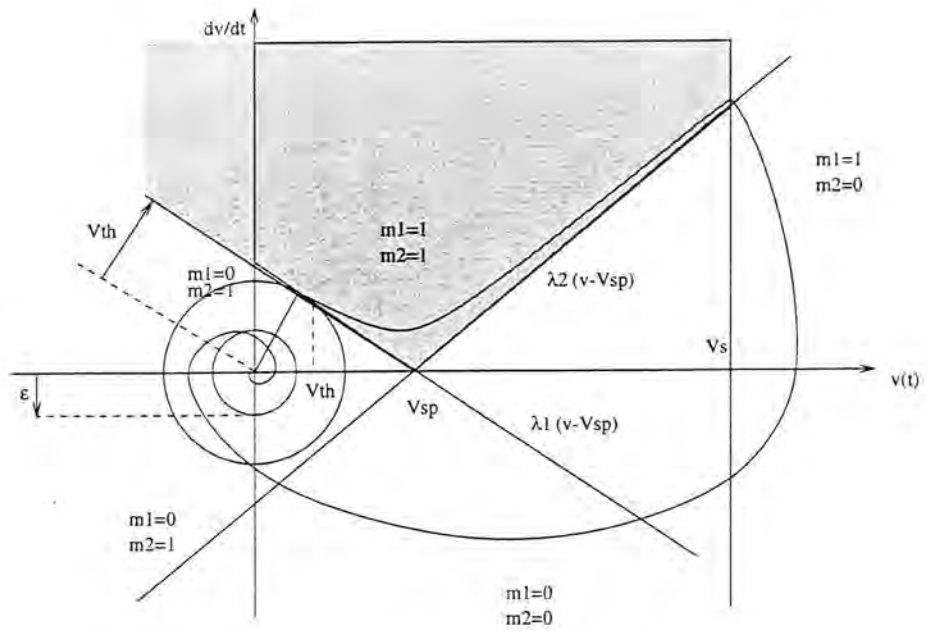

FIGURE 4.2: Phase plot illustration

Where $a_1 = a_2 = 2.5$ and $b_1 = b_2 = 2$ in this example. In the equations above the (-) sign as a subscript refers to the previous state of the corresponding quantity.

4.4. Results

The results depicted by figure 4.3 are obtained using the BLS-model coefficients calculated in section 4.5..

- Figure 4.3 shows different results for two different firing frequencies. The first two windows show the response of the model along with the train of impulses applied to it. These are of such a frequency that the recovery is attained before the application of the next impulse ($f_{in} = 62\,Hz$).

- Similarly, the second two windows show that there is no response to impulses applied before the membrane recovers from the previous excitation.

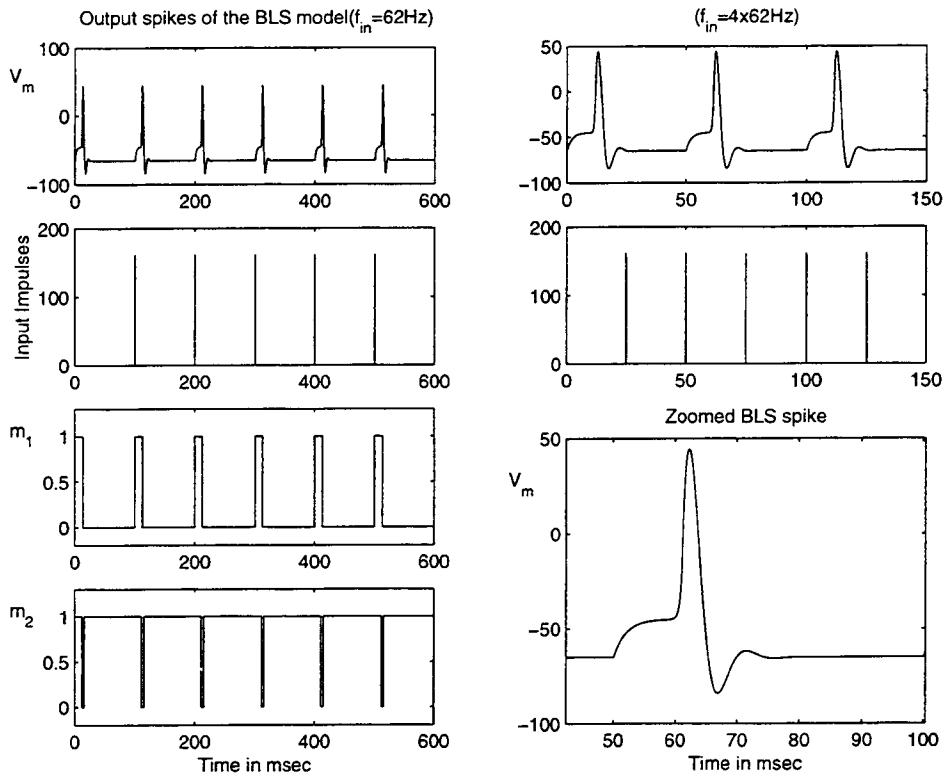

FIGURE 4.3: Time trajectories of the model output for different input frequencies

- The last window shows the zoomed spike for clarity.
- Finally, the two small windows in the lower left side of figure 4.3 show the control signals m_1 and m_2.

4.5. Coefficient Determination Based on The HH-Action Potential

4.5.1. *Stable Focus*

In this section, the features of the an action potential obtained from simulating the HH-model are explored in order to obtain the order of magnitudes of the bang-bang model parameters. Time response specifications of a second order system[17] are used here to

measure the settling time, T_s and the peak time [2] T_p of the spike portion which behaves as a stable focus.

The settling time, T_s is the time required for the output to settle to within a certain percent of its final value. The two commonly used values are 5 and 2 percent. Regardless of the percentage used, for the second-order undamped system, the settling time is directly proportional to the time constant τ[17]; that is,

$$T_s = k\tau = \frac{k}{\zeta\omega_n} \tag{4.7}$$

where k is determined by the defined percentage, ζ is the dimensionless damping ratio and ω_n is defined to be the natural frequency or the undamped frequency.

The peak time is given by

$$T_p = \frac{\pi}{\omega_n\sqrt{1-\zeta^2}} \tag{4.8}$$

Although equation 4.8 gives a peak value of the step response, the situation here is equivalent since the membrane potential falls from some initial conditions down to the equilibrium point.

Figure 4.4 shows a spike signal used to roughly determine the second order model coefficients of the stable focus.

Using matlab and assuming that the final value of V_m is V_{mf}, Ts is approximated as

$$T_s = \max_t \left(|V_m(t) - V_{mf}| \geq 2\,|V_{mf}|\,/100\right) \tag{4.9}$$

From figure 4.4 it is found that $T_s = 10.5248msec$ and that $T_p = 3msec$. From equations 4.8 and 4.7, ζ and ω_n are found to approximately be

$$\zeta = \frac{1}{\sqrt{1+\frac{\pi}{4}\frac{T_s}{T_p}}} \approx 0.3413 \tag{4.10}$$

$$\omega_n = \frac{4}{10.52\zeta} \approx 1.11 \tag{4.11}$$

[2] The time it takes for the spike to drop from its peak value to the apparent undershoot.

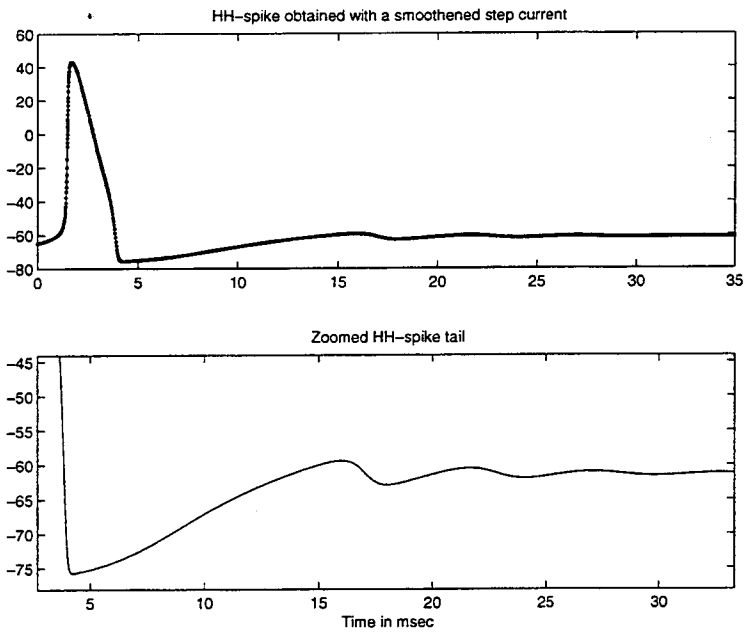

FIGURE 4.4: HH-spike used for a rough parameter determination.

4.5.2. *Saddle Point*

The rising part of the spike has a very high slope. It is possible to vary how fast the potential should increase by changing the slope of the eigen vector corresponding to the positive eigenvalue. However, since this is limited by the amount of overshoot produced by the stable focus after the switching occurs, the switching set point from the saddle point to the stable focus (V_{sp}) should be decreased every time the slope of the positive eigenvector is increased. The eigenvalues $\lambda_1 = 3$ and $\lambda_2 = -0.5$ produce the spike shown in figure 4.5

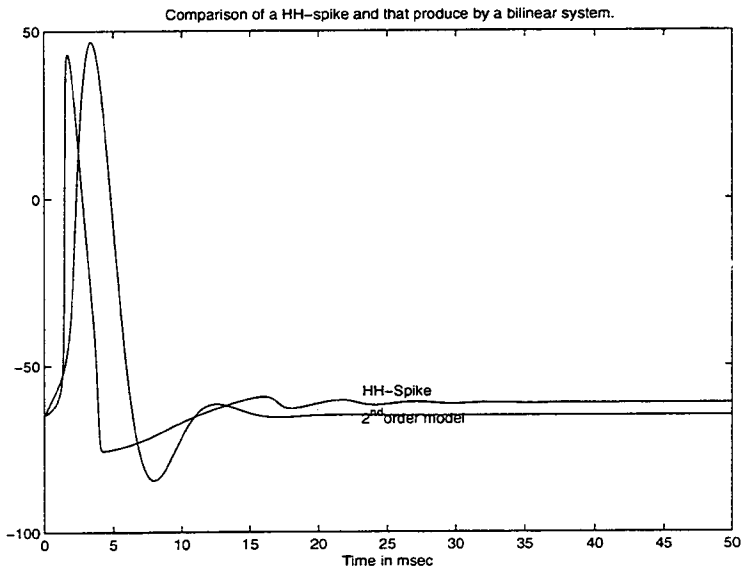

FIGURE 4.5: Comparison of the HH-spike and that produced by a bilinear system (fit not optimized).

4.6. Model Parameter Identification

4.6.1. *Recursive Parameter Identification Using RPM/RLS*

The problem at hand is to model the neuron using switching between different linear systems by a bang-bang controlled BLS. Each of these different linear systems is individually characterized by its own number of parameters depending on the state of the membrane and the type of ions the membrane is permeable to. These parameters should be optimally determined to best suit and represent the physical biological phenomena which characterize the neuron. HH-model is taken as a reference in this work.

There are numerous methods used to optimally identify systems' parameters, many of which are detailed in [18]. These methods differ from one another according to the kind of circumstances conditioned by the amount and the type of noise involved, how fast the signals vary etc.

Among the mostly used parameter estimation methods is the recursive least square method (RLS). This algorithm has many variants, thoroughly discussed in [18]. However, in order to use this method the system model is traditionally put in a linear form with respect to the parameters to be identified. An example of such a model is an ARMA model which is written as follows

$$\underline{y} = \Phi\underline{\theta} \tag{4.12}$$

where $\underline{y}$ is a vector of the measurements, $\underline{\theta}$ the system parameters to be determined and Φ the coefficient matrix usually formed from the history of both the measured output and the available input values. In our case, the piecewise linear systems are described by second-order differential equations whose parameters are to be identified.

In order to use one of the optimization algorithms, such as the least square method, to precisely identify the system coefficients to fit the HH-model, a means to convert the model differential equations to the form given by 4.12 is required.

A method called *Reinitialized Partial Moments (RPM)*, outlined in the appendix A, offers one tool to transform a differential equation model into a form given by equation 4.12.

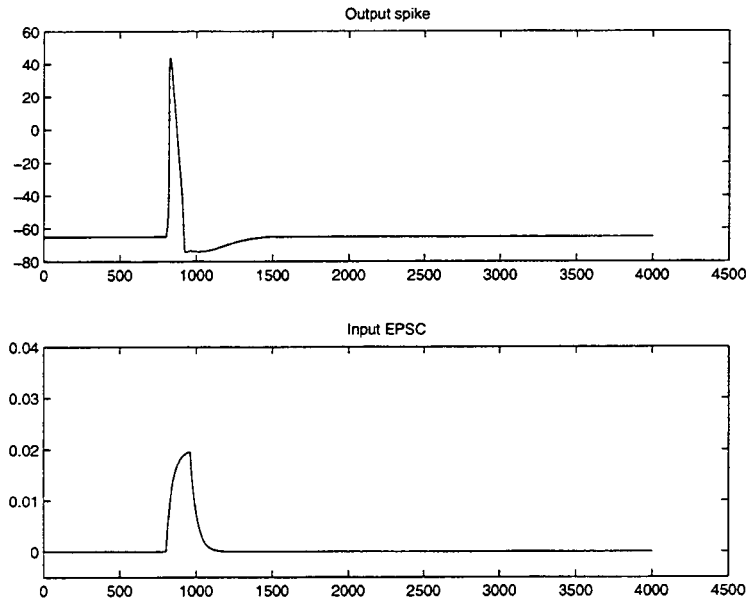

FIGURE 4.6: HH-neuron input and output for identification.

The parameter coefficients are integrals (instead of being derivatives) which are easily computed using one of numerical methods such as Simpson method.

The RPM method together with the recursive least square algorithm are used to identify the four parameters of a general second order differential equation 4.13, with a lead term, representing the model in order to inspect the parameter evolution throughout the whole spiking period.

$$\frac{d^2y(t)}{dt} + a_1\frac{dy(t)}{dt} + a_0y(t) = b_1\frac{du(t)}{dt} + b_0u(t) \tag{4.13}$$

The obtained results shown in figure 4.7, particularly a_0 and a_1 provide an insight about the variable structure property of the membrane impedance. It can be seen that after a brief moment during which a_0 and a_1 have different signs (saddle point) they remain relatively constant along two plateaus suggesting the existence of two different stable foci.

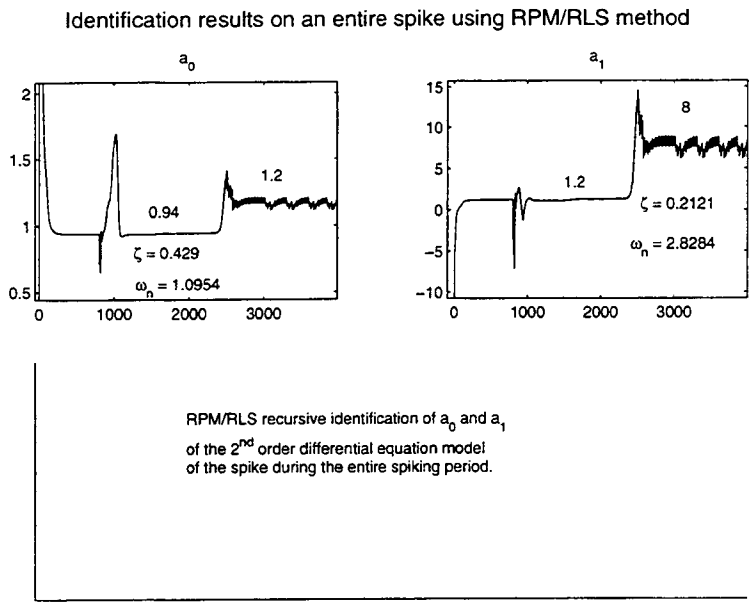

FIGURE 4.7: Identified four parameters throughout the spiking process using RPM/RLS method.

It is, however, hard to extract meaningful results for the eigenvalues, λ_1 and λ_2, corresponding to the saddle point of the system. The reason for this is that during the very brief period during which the potential rises rapidly (saddle point), there are very few data points and therefore the algorithm does not have enough time to converge to some meaningful values. Nevertheless, it can be noticed that a_0 and a_1 evolve being of opposite signs suggesting the saddle point structure.

4.6.2. *Optimal Parameter Determination of the Coefficients in the Three Spike Regions.*

In light of above discussion in section 4.6.1., the generated HH-model spike is divided into three regions. As shown in figure 4.8. The first part labeled $f_1(t)$ corresponds to the saddle point. The second and third portions labeled $f_2(t)$ and $f_3(t)$ are assumed to be

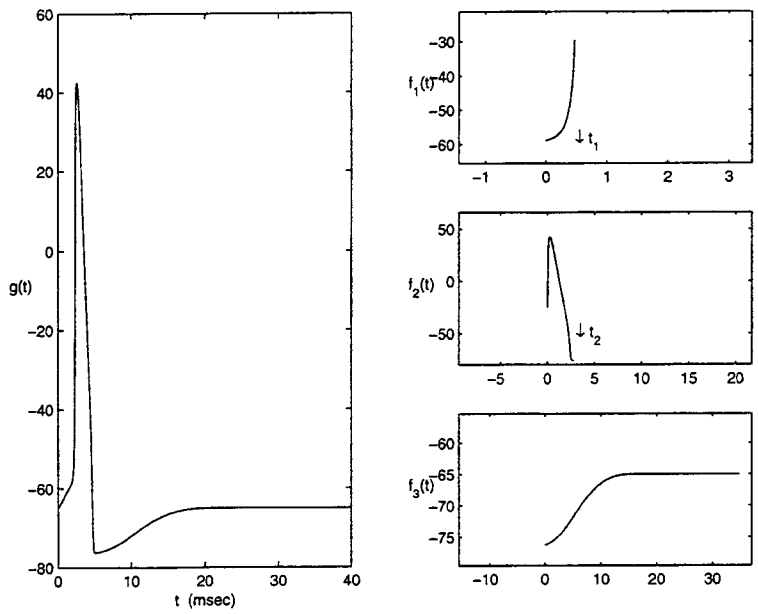

FIGURE 4.8: HH-neuron spike divided into three piecewise constant parameter regions.

generated by two different stable foci. The parameters are to be determined to fit these three portions in the least square sense.

As shown in section 3.4.3., a lead term included in the differential equation representing the resting potential equilibrium point ($f_3(t)$ in figure 4.8) advances or delays the occurrence of the spike. On the other hand, it is noted from simulations of the BLS-model that varying the threshold point above the negative eigenvalue as a function of the input impulse amplitude also delays or advances the spike generation. More simulations and validation of the model are required to determine the best method to generate the similar latency curves as those of the HH-mode. In any case for the purpose of this section, including a lead term in the resting stable focus is not relevant since the spike is generated by an impulse which ends by the time a threshold is reached. The whole spiking process evolves autonomously with a zero input.

If the three different spike regions are written with respect to 0 time reference, and if g(t) is the entire spike from the threshold, then

$$g(t) = f_1(t) + f_2(t - t_1) + f_3(t - t_1 - t_2) \tag{4.14}$$

with

$$\ddot{f}_1(t) + a_1\dot{f}_1(t) + a_0 f_1(t) = 0 \tag{4.15}$$

$$\ddot{f}_2(t) + a_1'\dot{f}_2(t) + a_0' f_2(t) = 0 \tag{4.16}$$

$$\ddot{f}_3(t) + a_1''\dot{f}_3(t) + a_0'' f_3(t) = 0 \tag{4.17}$$

$$\tag{4.18}$$

The solution of equation 4.15 is given as

$$f_1(t) = k_1 e^{\lambda_1 t} + k_2 e^{\lambda_2 t} \text{ with } f_1(t) = (v_m(t) - V_{sp}) \text{ for } 0 \leq t < t_1 \tag{4.19}$$

In this equation, the eigenvalues, λ_1;λ_2, the two constants k_1; k_2 and the saddle point location V_{sp} are to be determined using a nonlinear curve fitting algorithm based on the least square method.

Similarly, $f_2(t)$ and $f_3(t)$, the solutions of equations 4.16 and 4.17 have the same form given respectively by

$$f_2(t) = 2k' e^{\alpha' t}\cos(\beta' t + \theta'), \quad \text{with} \tag{4.20}$$

$$f_2(t - t_1) = (v_m(t) - V_{sf2}) \text{ for } t_1 \leq t < (t_1 + t_2) \quad \text{and}$$

$$f_3(t) = 2k'' e^{\alpha'' t}\cos(\beta'' t + \theta''), \quad \text{with} \tag{4.21}$$

$$f_3(t - (t_1 + t_2)) = (v_m(t) - V_{sf1}) \text{ for } t \geq (t_1 + t_2)$$

Where k', k'', α', α'', β', β'', V_{sf1} and V_{sf2} are also to be determined.

Saddle Point		Intermediate SF		Resting SF	
λ_1	1.5897	k'	216.6493	k''	8.9005
λ_2	17.2881	θ'	92.9522	θ''	14.8043
k_1	2.802	α'	-0.9724	α''	-0.1979
k_2	0.0002	β'	0.6175	β''	0.1759
V_{sp}	-62.6624	V_{sf2}	-105.1434	V_{sf1}	-65.0965
a_1	-18.8778	a_1'	1.9448	a_1''	0.3958
a_0	27.4828	a_0'	1.3269	a_0''	0.0701
		ζ'	0.8442	ζ''	0.7476
		ω_n'	1.1519	ω_n''	0.2647

TABLE 4.1: Optimal parameters for curve fitting the action potential in three regions

4.6.3. *Estimated Parameter Values*

Figure 4.9 shows both g(t) and the approximated version rebuilt using the parameters found in curve-fitting equations 4.19–4.21

It can easily be seen that by means of another stable focus, the HH-spike can be very closely approximated. In this situation, two switchings take place during the firing process of the membrane. Hence, the membrane state visits three regions in the state space after the spiking threshold is attained. At least two control variables are needed to distinguish the region of the current membrane state in the state space in order to change the membrane structure as its state switches from one region to the other. Depending on the the switching limits(during the spiking process), a logic circuit could be built to provide these variable.

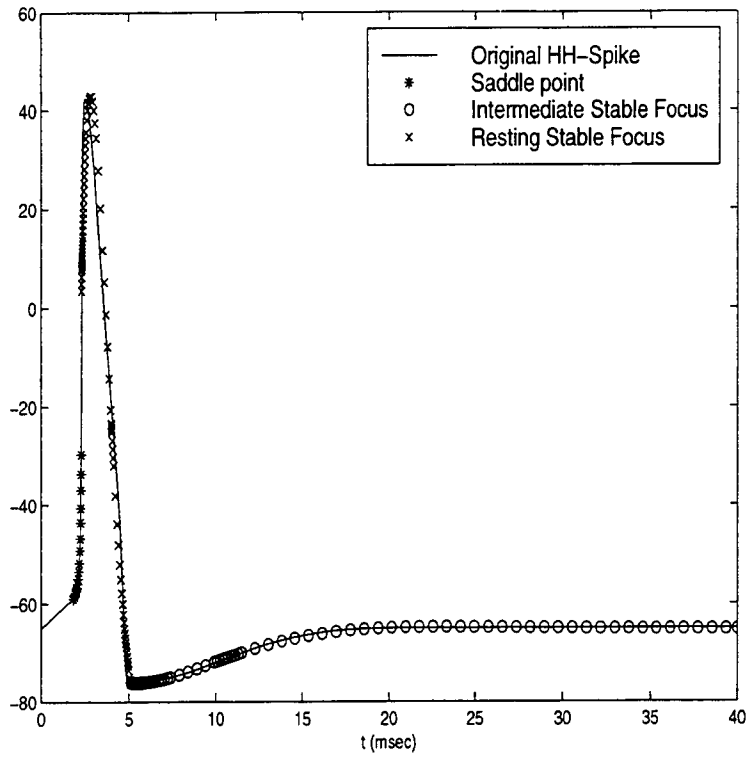

FIGURE 4.9: Superposition of the HH-spike with the reconstructed version using optimally determined parameters.

Assume the control variables u_1 and u_2 could take distinct values over the state space according to table 4.2. These values can be used together with the the coefficients a_i of each individual equation describing the structure in the corresponding state region and combine them into one differential equation. The resulting differential equation is called a bilinear differential equation.

Equations 4.15– 4.17 can, now, be combined into the following equation:

$$\begin{aligned} \frac{d^2 v_m}{dt^2} &+ \left[a_2 + u_1(a_1' - a_1) + u_2(a_1'' - a_1)\right] \frac{dv_m}{dt} \\ &+ \left[a_0 + u_1(a_0' - a_0) + u_2(a_0'' - a_0)\right] v_m \\ &- \left[a_0 V_{sp} + u_1(a_0' V_{sf1} - a_0 V_{sp}) + u_2(a_0'' V_{sf2} - a_0 V_{sp})\right] = 0 \end{aligned} \tag{4.22}$$

Region	u_2	u_1
Saddle Point	0	0
Intermediate SF	1	0
Resing SF	0	1

TABLE 4.2: Control variables for changing the membrane structure during the spiking process.

The state space representation of equation 4.22 is written bellow.

$$\begin{aligned}\dot{x} &= Ax + u_1 \begin{bmatrix} 0 & 0 \\ (a_0 - a_0') & (a_1 - a_1') \end{bmatrix} x + u_2 \begin{bmatrix} 0 & 0 \\ (a_0 - a_0'') & (a_1 - a_1'') \end{bmatrix} x \\ &- \begin{bmatrix} 0 \\ a_0 V_s p \end{bmatrix} - u_1 \begin{bmatrix} 0 \\ (a_0' - a_0 V_s p) \end{bmatrix} + u_2 \begin{bmatrix} 0 \\ (a_0'' - a_0 V_s p) \end{bmatrix} \end{aligned} \tag{4.23}$$

Equation 4.23 is under the following form:

$$\dot{x} = Ax + \sum_{i=1}^{2} u_i N_i x - c + \sum_{i=1}^{2} u_i c_i \tag{4.24}$$

Where

$$\begin{bmatrix} v_m & \dot{v}_m \end{bmatrix}^T,$$

$$A = \begin{bmatrix} 0 & 0 \\ a_0 & a_1 \end{bmatrix}, \quad N_1 = \begin{bmatrix} 0 & 0 \\ (a_0 - a_0') & (a_1 - a_1') \end{bmatrix}, \quad N_2 = \begin{bmatrix} 0 & 0 \\ (a_0 - a_0'') & (a_1 - a_1'') \end{bmatrix}$$

and

$$c = \begin{bmatrix} 0 \\ a_0 V_s p \end{bmatrix}, \quad c_1 = \begin{bmatrix} 0 \\ (a_0' - a_0 V_s p) \end{bmatrix}, \quad c_2 = \begin{bmatrix} 0 \\ (a_0'' - a_0 V_s p) \end{bmatrix}$$

V_{sp}, V_{sf1} and V_{sf2} are the the saddle point, resting and intermediate stable focus equilibrium points respectively.

Substituting the values listed in table 4.1 in the matrices above gives:

$$A = \begin{bmatrix} 0 & 1 \\ 27.5 & -18.9 \end{bmatrix}, \quad N_1 = \begin{bmatrix} 0 & 0 \\ 26.2 & -20.8 \end{bmatrix}, \quad N_2 = \begin{bmatrix} 0 & 0 \\ 27.4 & -19.3 \end{bmatrix},$$

and

$$c = \begin{bmatrix} 0 \\ -1722.1 \end{bmatrix}, \qquad c_1 = \begin{bmatrix} 0 \\ 1582.6 \end{bmatrix}, \qquad c_2 = \begin{bmatrix} 0 \\ 1717.6 \end{bmatrix}$$

Equation 4.24 is a bilinear system equation that describes the membrane. It implements the second order differential equation given by equation 3.18 with different channel resistance, inductance in different regions state space. The resting equilibrium stable focus could be interpreted as the state of the potassium channel. The saddle point on the other hand represents the sudden permeability change sodium channel. And finally, the intermediate stable focus represents the transition from one structure to the other, which involves the motion of both ion types through the membrane.

5. CONCLUSION AND PERSPECTIVE

It is seen that the bang-bang controlled bilinear model (BLS) provides a flexible manner to obtain a satisfactory approximation of the HH-model features. In addition to the fairly good approximation of the spike obtained from simulating the HH-model, the BLS-model is shown to inherit the characteristics which seem to be of a high importance in the transfer of information among different neurons. The first of these trades is the ability of the model to fire by producing an action potential as a response to an appropriate current excitation. While in the HH-model the firing threshold depends on the voltage level, in the BLS-model this depends on both the membrane voltage and its rate of change as the firing threshold is defined to be the negative slope line in figure 4.2. Also, note that the BLS model is flexible enough to approximate other species' neurons besides the squid giant axon for the HH model.

The second property is the refractoriness of the membrane. This characterizes the low sensitivity of the model to the input signals during the firing process. In the BLS-model, this feature is implemented by assuming two concentric circles around the resting stable focus in the state plane. When the magnitude of the model state is outside the outer circle and satisfies the firing condition (crossing the negative eigenvector) the input signal is completely attenuated. Only when the model state enters the inner circle is the input enabled again by being multiplied by a unity gain. This operation is performed by means of an ideal relay in the simulations of the BLS-model.

Finally, the property related to latency, concerns the study of the effects other afferent currents have on the spike occurrence time set by an excitatory post-synaptic current pulse (EPSC)[3]. Simulations done on the HH-model show that if the membrane is properly depolarized very near the threshold, the membrane potential either spikes or aborts by falling back to its resting potential after a long plateau around the threshold voltage. The same

[3]This is the current pulse presented to the membrane at some point in time. Its purpose is to depolarize the membrane near the threshold

behavior is shown by the BLS-model, in the sense that if the membrane state is brought by an appropriate excitation to lie exactly on the negative eigenvector switching line, the state would move to the saddle point equilibrium point, generating a similar plateau shape in the spike. Then any perturbation would either cause it to move towards the resting stable focus (aborted spike) or shoot up along the positive eigenvector producing a spike.

An approximation of the latency curves of the model could be obtained in two different ways. It is seen that if the threshold point is varied between two limits, above and near the negative slope eigenvector, according to the amplitude of the input signal, one can change the curvature (inflection point) of the action potential around the threshold. This curvature could be very long and flat before the voltage increases rapidly towards the sodium equilibrium potential. This happens when the switching occurs very close to the eigenvector just as described in the preceding paragraph. The farther the switching threshold from the eigenvector the faster the spike moves along the state trajectory in the saddle point region. This is all evident when considering the state space. This delay, which it takes for the spike to exceed its inflection point, is recorded against the presentation times of other input impulses and are called latency curves.

The other method could be to introduce a lead term (proportional plus derivative) as opposed to the way described above. This lead term is justified by the impedance plots shown in section 3.4.1. and the natural latency curves, shown in figure 3.12, of a simulated second-order system with a stable focus equilibrium point. This method remains to be detailed and pursued in future research.

It is important to mention that a certain number of improvements and modifications to the model remain to be done in order to improve dynamic accuracy. It would be desirable, in the future work, to use real data collected from a particular cell for optimal identification of its BLS model parameters, using one of the system identification techniques such as that outlined in appendix A.

In dealing with the refractoriness, as mentioned above, an ideal relay is assumed to perform the task described above. In reality, this happens a bit differently. Although the

disabling of the inputs occurs relatively faster, enabling happens progressively in an almost linear manner[4] This could be implemented assuming sigmoidal or linear variations of the gains and the attenuators of the input around the transitions of the refractory period. More work and simulations are to be performed in order to explain more precisely the dynamics of this gain variation and to better approximate it. Also, rather than using heavy-side switching of the parameters in a bang-bang fashion to change the membrane structure, the model could well be improved using smooth transitions (sigmoidal functions) from one value to another since such transitions are common to most biological processes. As such, the use of the intermediate stable focus to improve the spike shape approximation would likely not be necessary.

As a future work, it would be interesting to linearize the Hodgkin and Huxley equations around the equilibrium points. This will allow a comparative analysis of the BLS-model suggested here and the linearized HH-equations.

In section 3.4.2., a general form of a single channel is given. The values of the inductance and channel resistance which appear in the coefficients of equation 3.18 are different from one channel structure to another. Hence, as opposed to HH-model where existence of different channels is assumed, the BLS-model consists of only one equivalent channel whose characteristics (L and R) change depending on the state of the membrane (v_m and $\dot{v}_m$). Although the BLS-model offers a simpler perspective than the HH-model, their macroscopic behaviors are quite consistent. The three equilibrium points shown in the more accurate BLS-model are related to the ionic batteries included in the HH electrical equivalent circuit shown in figure 2.5. The change in the channel structure which is exclusively related to the membrane voltage and its rate of change can also be related to the biological reaction of the membrane to different types of ions involved in the current flow through the membrane. The simplicity of the BLS model, from the engineering point of view, constitute a very important aspect. Nowadays neural-networks form a basis for modern computers and artificial intelligence. Hence, Synthesizing a neuron is an unavoidable need to implement

[4]Linear increase of the gain from zero to a constant value.

such networks. The synthesis simplicity of BLS systems presents an ambition to construct integrated circuit neurons which would exhibit as many real neuron properties as possible as it is seen in this work.

BIBLIOGRAPHY

1. Hodgkin A. & Huxley A. F. A quantitative description of membrane current and its application to conduction and excitation in nerve. *J. Physiol. London, UK*, 117:500:544, 1952.

2. Anderson J. A. *An Introduction to Neural Networks.* MIT Press, Cambridge, UK, 1995.

3. Cole K. S. & Curtis H. J. Electric impedance of the squid giant axon during activity. *J. Gen. Physiol. NY,USA*, 24:649–670, 1939.

4. Hille B. Ionic basis of resting and action potentials. *Handbook of Physiology of The Nervous System*, I:99–136, 1997.

5. Edstrom J. L. & Mpitsos G. J. Relating linear membrane impedance to the timing between input currents and output action potentials in model neuron. *Biol. Cybern.(under review) Berlin, Germany*, 1999.

6. Trigeassou J. C. *Contribution à l'extention de la méthode des moments en automatique. Application à l'identification des systèmes.* Thèse de Doctorat Es. Science Poitiers, France, 1987.

7. Hodgkin A. L. & Huxley A. F. Action potentials recorded from inside a nerve fibre. *Nature, London, UK*, 144:710:711, 1939.

8. Hodgkin A. L. & Huxley A. F. Currents carried by sodium and potassium ions through the membrane of the giant axon of *loligo*. *J. Physiol. London, UK*, 116:449:472, 1952.

9. Hille B. *Ionic Channels of Excitable Membranes.* Sinauer Associates Inc. MA, USA, 1984.

10. Hodgkin A. L. & Huxley A. F. The components of membrane conductance in the giant axon of *loligo*. *J. Physiol. London, UK*, 116:473:496, 1952.

11. FitzHugh R. A kinetic model of the conductance changes in nerve membrane. *J. Cell. Comp. Physiol. PA, USA*, 66, suppl. 2:111:117, 1965.

12. FitzHugh R. Impulses and physiological states in theoretical models of nerve membrane. *Biophysical Journal, MD, USA*, 1:445:466, 1961.

13. FitzHugh R. Thresolds and plateaus in the hodgkin-huxley nerve equations. *J. Gen. Physiol. NY, USA*, 43:867:896, 1960.

14. Bower J. M. & Beeman Springer D. *The Book of Genesis: Exploring Realistic Models with the General Neural Simulation System.* Springer-Verlag Publisher. CA, USA, 1995.

15. Hodgkin A. L. & Huxley A. F. Ionic currents underlying activity in the membrane of the giant axon of the squid. *Arch. Sci. Physiol. Paris, France*, 3:129:150, 1949.

16. Mohler R. R. *Nonlinear Systems*, volume 2 (Application to Bilinear Control). Prentice-Hall, Englewood Cliffs N.J., USA, 1991.

17. Phillips L. C. & Harbor R. D. *Feed Back Control Systems.* Prentice Hall, N.J., USA, 1988.

18. Najim M. *Modelisation et identification en traitement de signal.* Masson, Paris, France, 1988.

19. Gerstein G. L. & Kiang Y.-S. An approach to the quantitative analysis of electrophysiological data from single neurons. *Biophysiological Journal, MD, USA*, 1:15:28, 1960.

20. Gimbarzevskey B. & Miura R. M. Quantification of membrane properties of trigeminal root ganglion neurons in guinea pigs. *J. Neurophysiol, MD, USA*, 55:995:1016, 1986.

21. Hodgkin A. L. The ionic basis of electrical activity in nerve and muscle. *Biol. Rev. Cambridge, UK*, 26:339:409, 1951.

22. Hodgkin A. L. Ionic movements and electrical activity in giant nerve fibres. *Proc. Roy. Soc. London, UK*, B 148:1:37, 1958.

23. Hodgkin A. L. & Horowicz P. The influence of potasium and chloride ions on the membrane potential of single muscle fibres. *J. Physiol. London, UK*, 148:127:160, 1959.

24. Hodgkin A. L. & Horowicz P. The effect of sudden changes in ionic concentrations on the membrane potential of single muscle fibres. *J. Physiol. London, UK*, 153:370:385, 1960.

25. Hodgkin A. L. & Huxley A. F. Measurement of current-voltage relations in the membrane of the giant axon of loligo. *J. Physiol. London, UK*, 116:424:448, 1952.

26. Hodgkin A. L. & Katz B. Ionic currents underlying activity in the giant axon of the squid. *Arch. Sci. Physiol. Paris, France*, 3:129–150, 1949.

27. Huxley A. F. & Stampfli R. Direct determination of membrane resting potential and action potential in single myelinated nerve fibres. *J. Physiol. London, UK*, 112:476:495, 1951.

28. Judd K. T. & Aihara K. Pulse propagation networks: A neural network model that uses temporal coding by action potentials. *Neural Networks, Oxon, UK*, 6:203:215, 1993.

29. Kenneth S. C. An analysis of the membrane potential along a clamped squid axon. *Biophysical Journal, MD, USA*, 1:401:418, 1961.

30. Kenneth S. C. & Moore J. W. Potassium ion current in the squid giant axon: Dynamic characteristic. *Biophysical Journal, MD, USA*, 1:1:13, 1960.

31. Lamport L. *LaTeX A Document Preperation System.* Addison-Wesley Publishing Company, MA, USA, 1986.

32. Mac Gregor R. J. *Neural and Brain Modeling.* Academic Press Inc. CA, USA, 1983.

33. Mohler R. R. *Nonlinear Systems*, volume 1(Dynamics and Control). Prentice Hall, Englewood Cliffs, NJ, USA, 1987.

34. Schwan. *Biological Engineering,Inter-University Electronic series*, volume 9. McGraw-Hill Company, NY, USA, 1969.

35. Coirault P. *Etude de la précision déterministe des méthodes d'identification des systèmes continus.* Thèse de Doctorat Es. Science Poitiers, France, 1992.

36. Schwarzenbach J. & Gill K. F. *System Modeling and Control, Second Edition.* Edward Arnold, London, UK, 1984.

Appendices

A Continuous System Identification

The least square method is extensively used in optimal parameter identification. It is suitable for the models that are linear with respect to the parameters such as the difference equation models in discrete systems. In the case of continuous systems described by differential equations, the coefficients of the parameters to be identified are derivatives of the outputs and/or inputs. The RPM method allows converting a differential equation to an integral equation and convert the coefficients from derivatives to integrals. These are easily computed using numerical integration such as Simpson or trapezoidal algorithms. This makes it, finally, possible to transform the differential equation to the form of equation 4.12, which is convenient to be used with the recursive least square method (RLS). The RPM method is outlined in this appendix.

A1. *Partial Moments Method*

Definition: Moments of a bounded function:

By definition, an n-order moment of a bounded function $f(t)$ is given by[6]

$$A_n(f) = \int_0^\infty \frac{t^n}{n!} f(t)dt \tag{5.1}$$

and an n-order partial moment is given by

$$A_{n,T}(f) = \int_0^T \frac{t^n}{n!} f(t)dt \tag{5.2}$$

Moment method: Principles of the method:

This method is best explained with a simple example. Assume that we have the following first order differential equation,

$$\frac{dy}{dt} = -a_0 y(t) + b_0 u(t) \tag{5.3}$$

Multiplication of equation 5.3 by t along with integrating along the interval [0 T] results in

$$\int_0^T t\frac{dy}{dt}dt = -a_0 \int_0^T ty(t)dt + b_0 \int_0^T tu(t)dt \tag{5.4}$$

Hence,

$$y(T) = -a_0 \frac{\int_0^T ty(t)dt}{T} + b_0 \frac{\int_0^T tu(t)dt}{T} + \frac{\int_0^T y(t)dt}{T} \tag{5.5}$$

Note that equation 5.5 is a linear model with respect to the desired unknown parameters, suitable for use with an RLS estimation algorithm.

$$y(T) = a_0\alpha_{0,T}(y) + b_0\beta_{0,T}(y) + \alpha_{1,T}(y) \tag{5.6}$$

$$= \underline{\varphi}^T(T)\underline{\theta} + \alpha_{1,T}(y) \tag{5.7}$$

With $\underline{\theta} = \begin{bmatrix} a_0 \\ b_0 \end{bmatrix}$ and $\underline{\varphi}^T(T) = [\alpha_{0,T}(y) \quad b_0\beta_{0,T}(y)]$

A2. ***Output Model Properties***

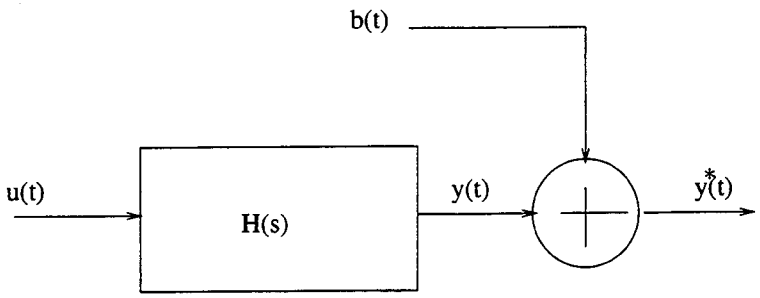

FIGURE 5.1: Output model of a system H(s)

In figure 5.1, the data are sampled at a period h *sec/sample*. The period T used in the integration above is then $T = kh$, where k is an integer.

The measurable output in figure 5.1, the membrane potential in the neuron case, is contaminated by a noise $b(t)$. This noise is the result of all the factors affecting the measurements such as uncertainties, acquisition tools' tolerances and etc. Since these contaminated

measurements are used to compute the vector $\underline{\varphi}$ above, the estimated outputs, $\hat{y}$ are written as follows;

$$\hat{y} = a_0\alpha_{0,T}(y^*) + b_0\beta_{0,T}(u) + \alpha_{1,T}(y^*) \quad (5.8)$$

$$= a_0\alpha_{0,T}(y) + b_0\beta_{0,T}(u) + \alpha_{1,T}(y) + e(T) \quad (5.9)$$

$$\text{where } e(T) = a_0\alpha_{0,T}(b) + \alpha_{1,T}(b) \text{ is the estimation error.}$$

$\hat{x}$ refers to the estimated values whereas x^* refers to the measured values. It can be shown[6] that the variance of $\{e_k\}$ is minimal for a properly chosen integration interval $T = K_{opt}h$, if $b(t)$, is a centered white noise. For a first-order system, it can be shown that $K_{opt} = \frac{\sqrt{3}}{a_0 h}\tau$ with τ being the system's time constant. The variance of the error of estimation of $\hat{y}(T)$ is then minimum when $T = T_{opt} = K_{opt}h$. This is illustrated in figure 5.2.

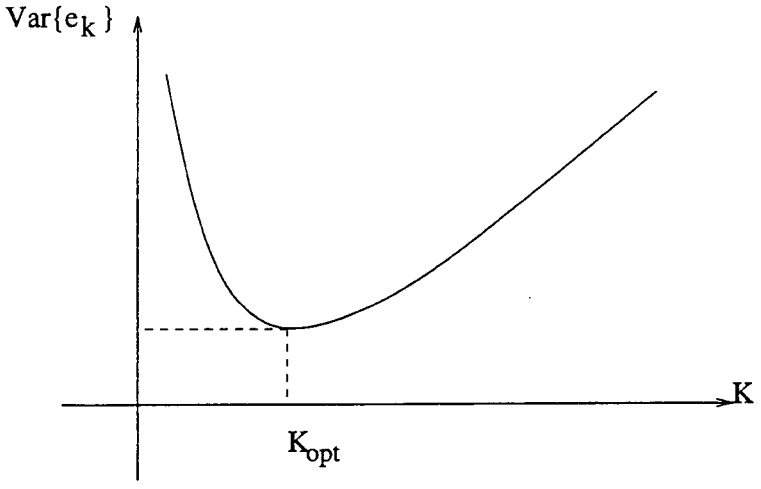

FIGURE 5.2: Variance of the estimation error vs K[6]

A3. *Reinitialized Partial Moments*

It is can also be shown that the estimation error minimum variance property is conserved when working on a mobile horizon $[0\ T]$. In other words, we reinitialize the moment computation at each instant $t = kh$. This idea is portrayed in figure 5.3

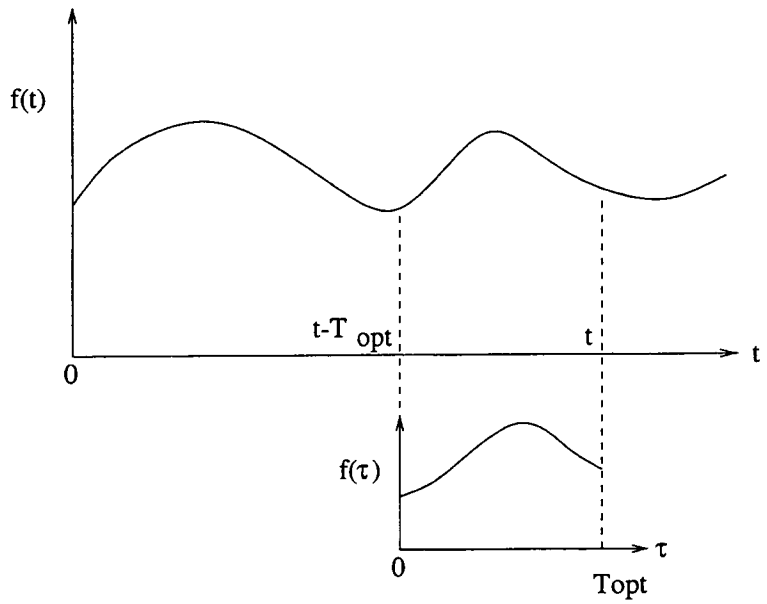

FIGURE 5.3: Mobile horizon in the reinitialized partial moment computation.[6]

We define then an **n-order reinitialized partial moment** of a function $f(t)$ on the interval $[t - T_{opt}; t]$ by

$$A_{n,t}(f) = \int_0^{T_{opt}} \frac{\tau^n}{n!} f(t - T_{opt} + \tau)dt \tag{5.10}$$

A4. *Reinitialized Partial Moment Model (first-order system)*

$$y(t) = a_0\alpha_{0,t}(y) + b_0\beta_{0,t}(y) + \alpha_{1,t}(y) \tag{5.11}$$

(5.12)

$$\alpha_{0,t}(y) = -\frac{A_{1,t}(y)}{T_{opt}} = \frac{-\int_0^{T_{opt}} \tau y(t - T_{opt} + \tau)}{T_{opt}} d\tau \tag{5.13}$$

$$= -\int_0^{T_{opt}} f_0(\tau) y(t - T_{opt} + \tau) d\tau \tag{5.14}$$

$$\alpha_{1,t}(y) = +\frac{A_{0,t}(y)}{T_{opt}} = \frac{\int_0^{T_{opt}} y(t - T_{opt} + \tau)}{T_{opt}} d\tau \tag{5.15}$$

$$= -\int_0^{T_{opt}} f_1(\tau) y(t - T_{opt} + \tau) d\tau \tag{5.16}$$

$$\beta_{0,t}(u) = +\frac{A_{1,t}(u)}{T_{opt}} = \frac{\int_0^{T_{opt}} \tau u(t - T_{opt} + \tau)}{T_{opt}} d\tau \tag{5.17}$$

$$= \int_0^{T_{opt}} f_0(\tau) u(t - T_{opt} + \tau) d\tau \tag{5.18}$$

In the previous set of equations, $f_0(\tau) = \frac{\tau}{T_{opt}}$, $f_1(\tau) = -\frac{1}{T_{opt}}$

A5. *Generalization to Order N*

$$H(s) = \frac{b_0 + b_2 s^2 + \cdots + b_M s^M}{a_0 + a_1 s + \cdots + a_{N-1} s^{N-1} + s^N}$$

For a general N-order linear differential equation model,

$$y^{(N)}(t) + \sum_{i=0}^{N-1} a_i y^{(i)}(t) = \sum_{i=0}^{M} b_i u^{(j)}(t) \tag{5.19}$$

the corresponding RPM (linear with respect to parameters) is given by

$$y(t) = \sum_{0}^{N-1} a_n \alpha_{n,t}(y) + \sum_{0}^{M} b_m \beta_{m,t}(u) + \alpha_{N,t}(y) \tag{5.20}$$

$a_n\alpha_{n,t}(y)$ and $b_m\beta_{m,t}(u)$ are functions of reinitialized partial moments of y and u. They are computed by using Simpson's method to evaluate the integrals given in 5.25.

A6. *Weighing functions*

$$f_0 = \frac{\tau^N (T_{opt} - \tau)^{N-1}}{(N-1)! T_{opt}} \tag{5.21}$$

$$f_i(\tau) = (-1)^i \frac{d^i f_0}{d\tau^i} \tag{5.22}$$

$$\alpha_{n,t}(y) = -\int_0^{T_{opt}} f_n(\tau) y(t - T_{opt} + \tau) d\tau \quad 1 \leq n \leq N \tag{5.23}$$

$$\beta_{m,t}(y) = +\int_0^{T_{opt}} f_m(\tau) u(t - T_{opt} + \tau) d\tau \quad 1 \leq m \leq M \tag{5.24}$$

$$\tag{5.25}$$

A7. *Recursive Least Square Method*

For a system modeled by equation 4.12, we use the measurements of y to form the following

$$\begin{pmatrix} y(k) \\ \vdots \\ y(k-N) \end{pmatrix} = \begin{pmatrix} \underline{\varphi}^T(k) \\ \vdots \\ \underline{\varphi}^T(k-N) \end{pmatrix} \underline{\theta} + \begin{pmatrix} e(k) \\ \vdots \\ e(k-N) \end{pmatrix} \tag{5.26}$$

The RLS algorithm is summarized by the following three equations. The details of this method could be found in[18].

$$\hat{\underline{\theta}}_{N+1} = \hat{\underline{\theta}}_N + K_{N+1} \left(y_{N+1} - \underline{\varphi}_{N+1}^T \hat{\underline{\theta}}_N \right) \tag{5.27}$$

$$K_{N+1} = P_N \underline{\varphi}_{N+1} \left[1 + \underline{\varphi}_{N+1}^T P_N \underline{\varphi}_{N+1} \right]^{-1} \tag{5.28}$$

$$P_{N+1} = \left[I - K_{N+1} \underline{\varphi}_{N+1}^T \right] P_N \tag{5.29}$$

Determining P_N allows the computation of K_{N+1} and the the estimation $\underline{\theta}$ at the instant $N+1$. This, of course assumes knowledge, or at least choosing $P(0)$ and $\hat{\underline{\theta}}(0)$.

A8. *Example of Parameter Identification On a Second Order System*

Figure 5.4 shows a simulation set up in order to demonstrate the usefulness of the RPM-method in identifying the parameters of a system whose inputs and outputs are recorded. The system has been arbitrarily chosen as shown in a *simulink* diagram. The statistical testing should therefore confirm the values shown in the transfer function block diagram.

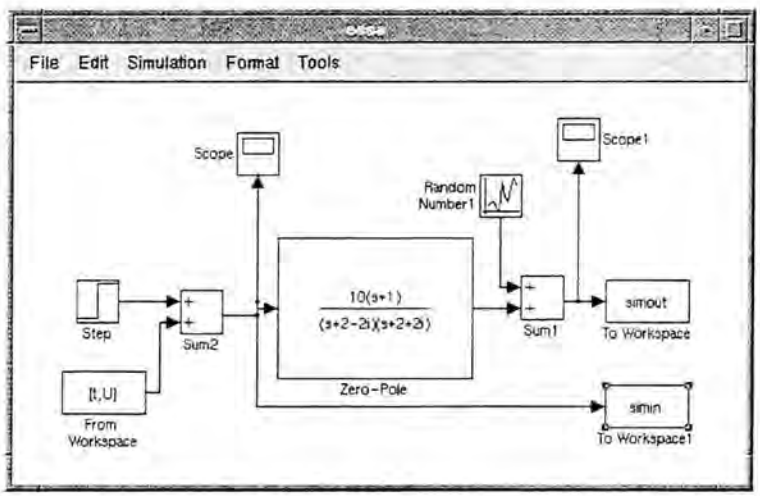

FIGURE 5.4: Simulation set-up for system identification

It is assumed that most of disturbances are mapped to the output just as depicted by figure 5.4. Figure 5.5 shows a sample trace of the output response of the system in the presence of noise for a nominally constant input.

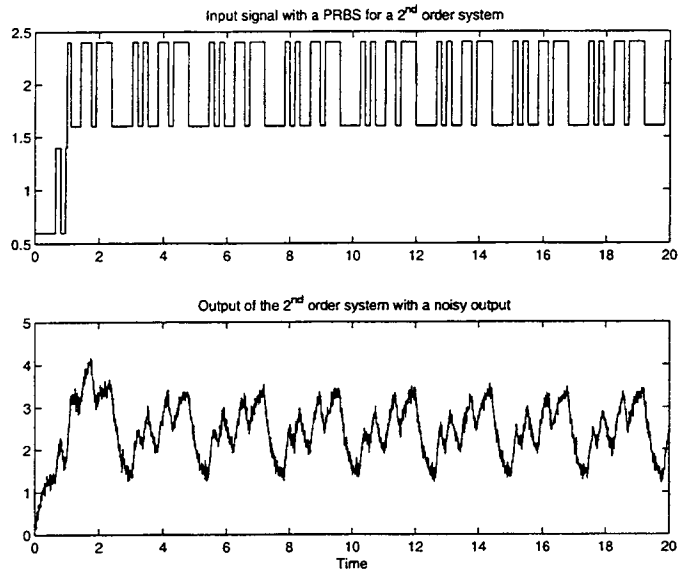

FIGURE 5.5: Step input with a PRBS and the system output

The noise variance and mean have been arbitrarily chosen to be 0.01 and 0 respectively. A PRBS[5], obtained, using *identinput* matlab command, is added to the step input to constitute an input excitation for system identification. The bit interval and the sequence length can be chosen on the basis of a preliminary estimate of the order of magnitude of the dominant roots of a system[36]. Figure 5.6 shows the identified parameters. It can be seen that they are pretty much close to those shown in the transfer function block in figure 5.4. The two responses of the system with both the original and the identified parameters are shown in figure 5.7

[5]Psoeudo Random Binary Sequence

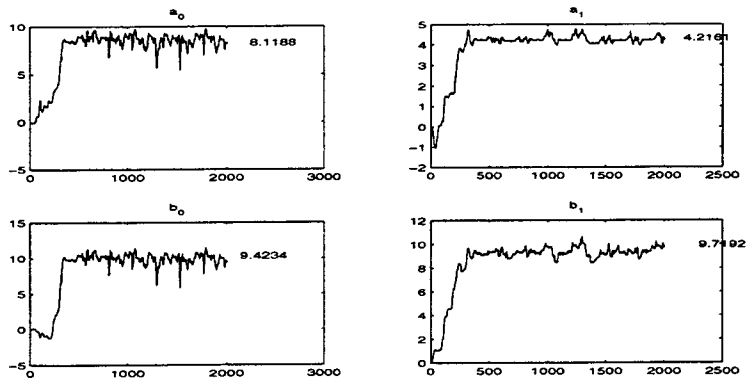

FIGURE 5.6: The 4 identified parameters.

A9. *Matlab Programs for RPM/RLS Computations*

This section shows matlab programs used in the RPM/RLS calculations

```
% ****************************************************************
%       function I = simpson(h,f)                                 *
%       This function implements Simpson Integration method.     *
%       Its arguments are :                                       *
%       h: sampling period.                                       *
%       f: Is either a row of an odd number of elements           *
%          or an array of rows of an odd n# of elements           *
%         (in order to have an even number of intervals)          *
%               Written by Y. Yahiaoui                            *
%                     05-09-1999                                  *
% ****************************************************************
```

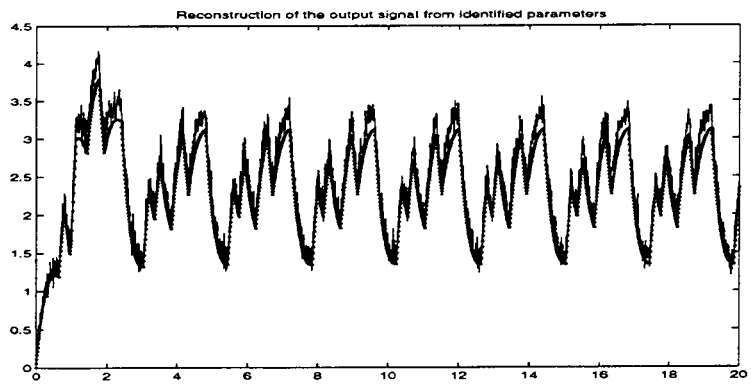

FIGURE 5.7: Output reconstructed using the identified parameters. It is superposed on the original contaminated output signal.

```
function I = simpson(h,f)


L = size(f,2);
I = h/3*(f(:,1)+f(:,L) + 4*(sum(f(:,2:2:L-1),2))+...
                        2*(sum(f(:,3:2:L-2),2)));
% ****************************************************************
%       function theta = mcr(y,H,par)                             *
%       This function implements the Recursive Least Square      *
%       Method(RLS).                                              *
%       This function takes                                       *
%       y: Nx1 measured values y.                                 *
%       H: Explicative NxM matrix H.                              *
%       par: Mx1 intial guess of the parameters.                  *
%               Written by Y. Yahiaoui                            *
%                   On May 9th 1999.                              *
% ****************************************************************
```

```
function theta = mcr(y,H,par)
dim = size(H); y = y(:);  % make sure to put y in a column vector.
  if  (dim(2) ~= length(par)) | (dim(1) ~= length(y))
      disp('Dimension problem Error, y(nx1)=H(nxm).par(mx1)!!')
  end
% Choice of P0 and Par0
I  = eye(dim(2),dim(2)); PN = I; theta(:,1) = par;
% Recursive Least Square Method.
  for i = 1:dim(1);
        K = PN*H(i,:)'*inv(1+H(i,:)*PN*H(i,:)');
        PN = (I - K*H(i,:))*PN;
        par = par + K*(y(i)-H(i,:)*par);
        theta(:,i+1) = par;
  end
% ****************************************************************
%              function H = windows(l,y)                          *
% This function takes a 1xN row and produces an (N-l+1)xl         *
% matrix whos rows are values seen through l-wide window.         *
%               Written by Youcef Yahiaoui                        *
%                       05-09-1999                                *
% ****************************************************************
function H = windows(l,y)
 if size(y,1) ~= 1  % make sure y is a row vector.
        y = y';
 end
N = length(y);
 for i = 1:l
     H(:,i) = y([1:N-l+1]+i-1)';
 end
```

A10. *First Implementation of RPM/MCR method*

```
% ***************************************************************
% function theta = mpr_mcr_ver2(T,u,y,Kopt,par0)                 *
% This function implements RPM/RLS method for continuous         *
% system identification.                                         *
%   T: Sampling Period                                           *
%   u: Input signal                                              *
%   y: Measurement vector                                        *
%   Kopt: optimum Reinitialization interval length Topt=Kopt*T   *
%   par0: Initial guess of the parameter vector                  *
%               Written by Youcef Yahiaoui                       *
%                   on 05-09-1999                                *

function theta = mpr_mcr_ver2(T,u,y,Kopt,par0)
y    = y(:)';  % Making sure that y is a column vector.
u    = u(:)';  par0 = par0(:);
tau  = 0:T:Kopt*T; % Reinitialization interval.
Topt = Kopt*T;     % Reinitialization period.
% Wheighing function computation.
f0   = tau.^2-(tau.^3)/Topt;    % Weighting function f0
f1   = 3*(tau.^2/Topt)-2*tau;   % Weighting function f1
f2   = 2-6*tau/Topt;            % Weighting function f2
% Least Square Algorithm.
dim = length(par0);
I  = eye(dim,dim);
PN = I;                         % Correlation Matrix
theta(:,1) = par0;              % Parameter Initialization
```

```
buffer = zeros(1,Kopt);          % Padding the measurets with 0's.
y = [buffer y];
u = [buffer u];
L = length(y);
lamda = 0.98;                    % Forgetting factor
% ~~~~~~~~~~    Implementation of the RPM method ~~~~~~~~~~~~~
  for i = Kopt+1:L
        alpha0 = -simpson(T,f0.*y(i-Kopt+(0:Kopt)));
        alpha1 = -simpson(T,f1.*y(i-Kopt+(0:Kopt)));
        alpha2 = -simpson(T,f2.*y(i-Kopt+(0:Kopt)));
        beta0  =  simpson(T,f0.*u(i-Kopt+(0:Kopt)));
        beta1  =  simpson(T,f1.*u(i-Kopt+(0:Kopt)));
% ~~~~~~~~~~   Implementation of the RLS algorithm ~~~~~~~~~~~
        h = [alpha0 alpha1 beta0 beta1];
        ynew = y(i)-alpha2;
        K = PN*h'/(lamda+h*PN*h');
        theta(:,i-Kopt+1) = theta(:,i-Kopt)+K*(ynew-h*theta(:,i-Kopt));
        PN = (I-K*h)*PN/lamda;
  end
% plotting the results
figure(22)
  for i = 1:4
      subplot(2,2,i);plot(theta(i,:))
      if i>2
         title(['b_',num2str(i-3)])
         else title(['a_',num2str(i-1)])
      end
  end
```

A11. *Second Implementation of the RPM/RLS Algorithm*

```
% ***************************************************************
% function parameters = mpr_mcr(Kopt,par0)                      *
% This program forms an MPR model for the second-order          *
% differential equation. It transforms the continuous           *
% second-order differential equation to a form                  *
% Y  = Phi(y)*theta,  using Reinitialized Partial Moments of y. *
% and it calls mcr function to estimate the parameters.         *
% Kopt: width of the moving window for the MPR                  *
% par0: Initial guess of the parameters.                        *
function parameters = mpr_mcr(time,in,out,Kopt,par0)
h = time(2)-time(1); Topt = Kopt*h;
v = out; n = length(v);
iex = in; tau = (0:h:Topt);
l = length(tau);
% Transforming v's to a matrix Hv
Hv = windows(l,v(1:n-1));
Hiex = windows(l,iex(1:n-1));
f0 = tau.^2-tau.^3/Topt;
f1 = 3*tau.^2/Topt-2*tau;
f2 = 6*tau/Topt - 2;
alpha_0s = -simpson(h,Hv*diag(f0));
alpha_1s = -simpson(h,Hv*diag(f1));
alpha_2s = -simpson(h,Hv*diag(f2));
beta_0s  =  simpson(h,Hiex*diag(f0));
beta_1s  =  simpson(h,Hiex*diag(f1));
% Explicative Matrix
H = [alpha_0s alpha_1s beta_0s beta_1s];
```

```
y = v(l+1:n); y = y(:);
y = y-alpha_2s;
parameters = mcr(y,H,par0(:));
% Plotting the results.
figure(22)
for i = 1:4
subplot(2,2,i);plot(time(1:length(parameters)),parameters(i,:))
   if i>2
      title(['b_',num2str(i-3)])

   else title(['a_',num2str(i-1)])
   end
end
```

B Latency Curves From a Stable Focus System with a Lead Term

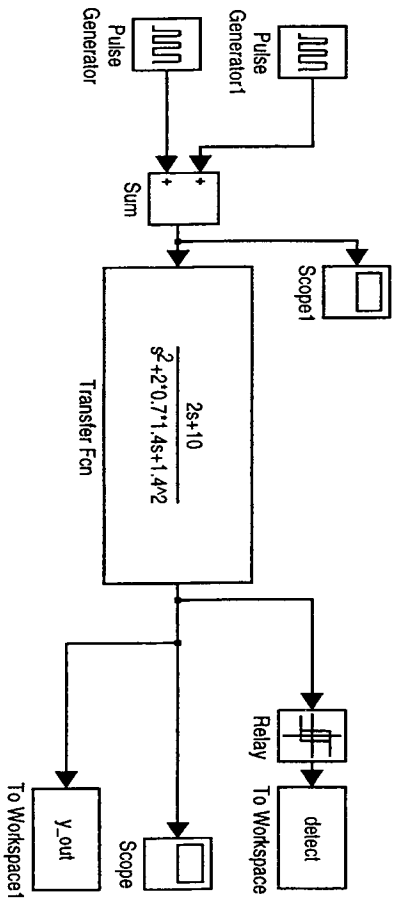

FIGURE 5.8: Latency Simulation Setup

B1. Simulation Driver Program:

```
% ************************************************************
% This program drives the simulink model to purturb a response *
% of a second order system to an input pulse.  This is done by *
% varying both the amplitude and presentation time of perturb- *
% impulses presented prior to the main input pulse.            *
%                 Written by Youcef Yahiaoui                   *
%                 on 07/27/1999 at 12:21 AM.                   *
% ************************************************************
clear
tt = [0:0.5:25];            % presentation times
A = [1.5:-0.5: -1.5];       % Amplitudes of the perturbing impulses.
L = length(A);
for k=1:L                   % Varying the perturbing impulse amplit$
   Ai = A(k);
   disp(['This is for Amplitude A_i = ', num2str(Ai)])
   for i=1:length(tt) % Presenetation time variation
      i
      ti =tt(i);
      tsim = [0:0.001:20];
      [t,x,y] = sim('ts',tsim);
      R =min(find(detect>0)); % Vout > preset_threshold detection
      Li(k,i) =tsim(R)                  % Recording the latency.
   end
end
save latency Li % Save the latency into a mat-file and print it
                % against the presentation times tt.
```

B2. Simulation Parameters: Solver Icon

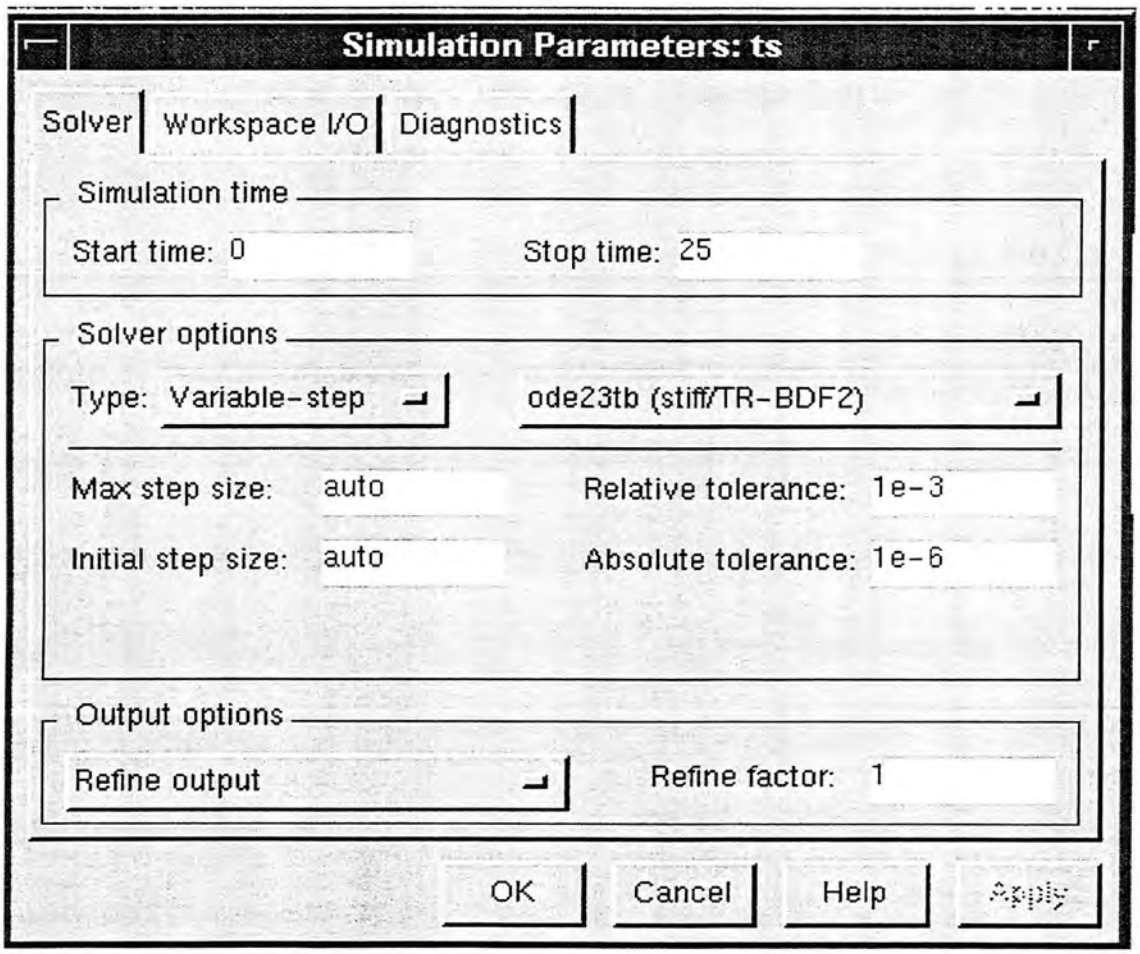

FIGURE 5.9: Simulation Parameters: Solver

B3. Simulation Parameters: Workspace Icon

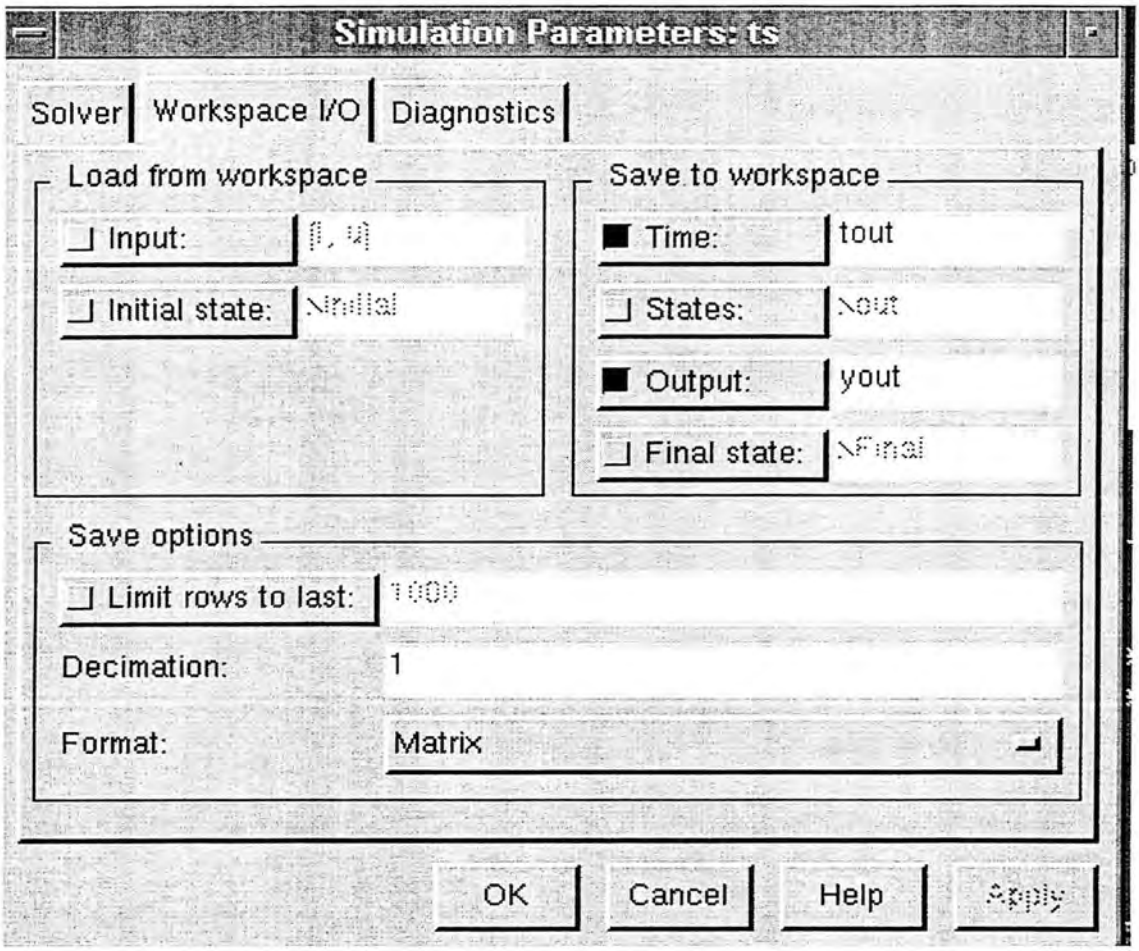

FIGURE 5.10: Simulation Parameters: Workspace.

B4. Relay Block:

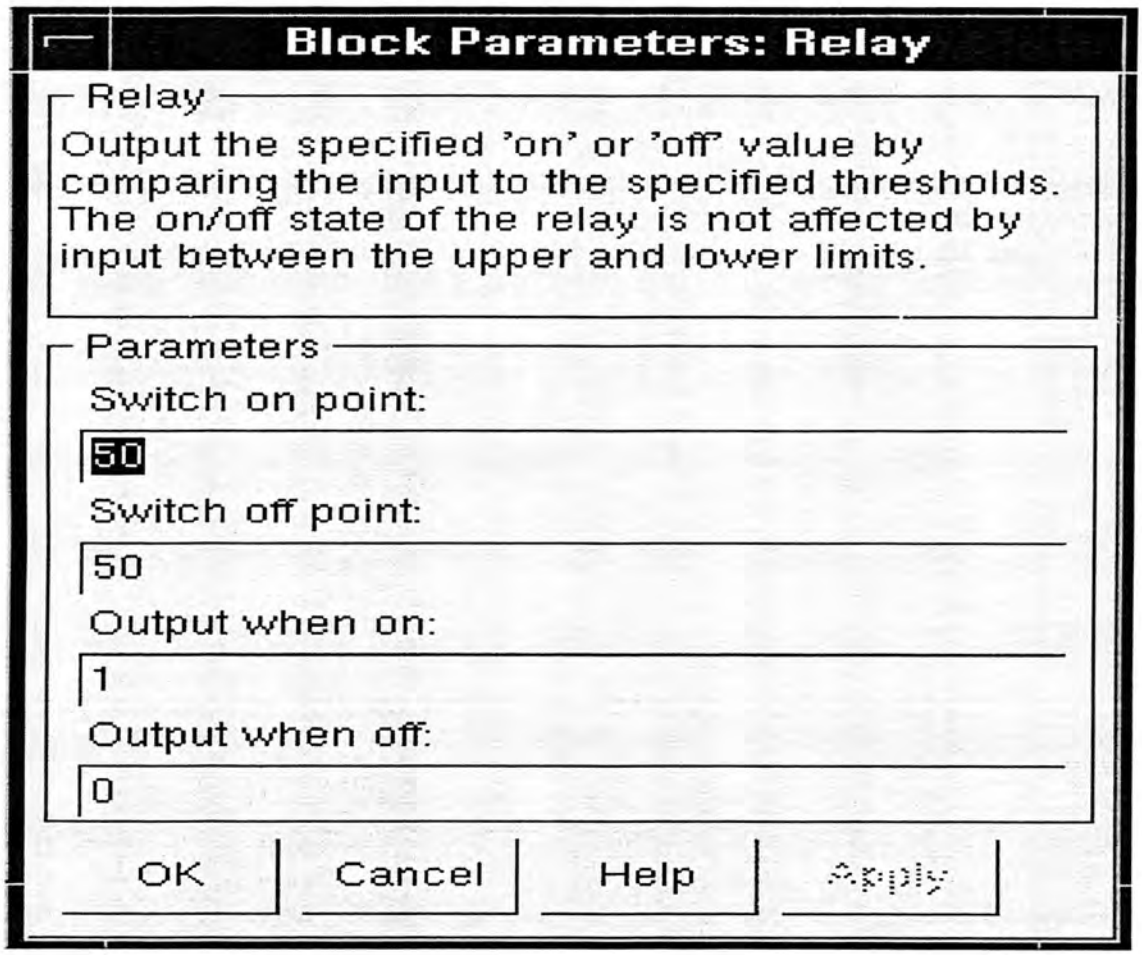

FIGURE 5.11: Simulation relay block

B5. Simulation Pulse Generator(Input Secondary pulses):

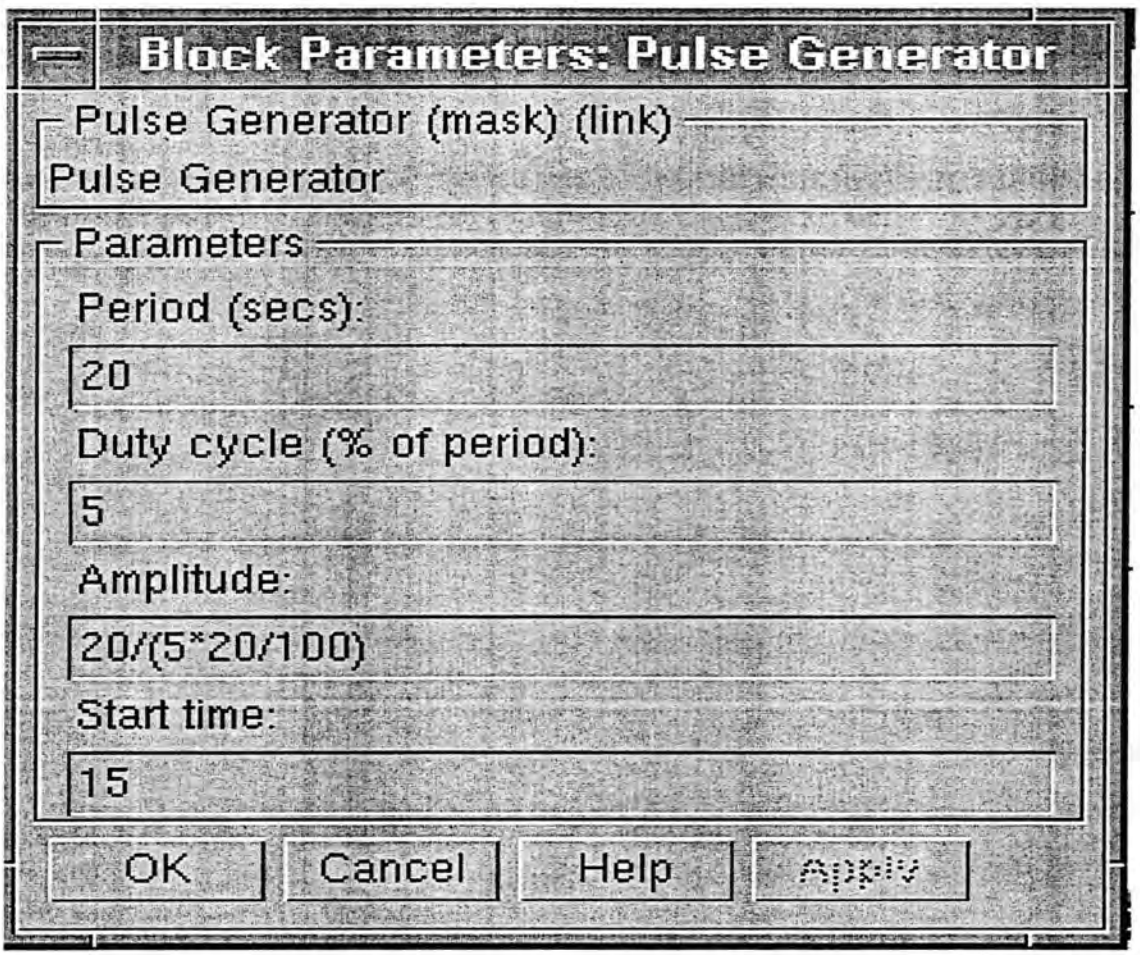

FIGURE 5.12: Simulation Pulse Generator(Input Primary Pulse):

B6. Simulation Pulse Generator1(Input Secondary pulses):

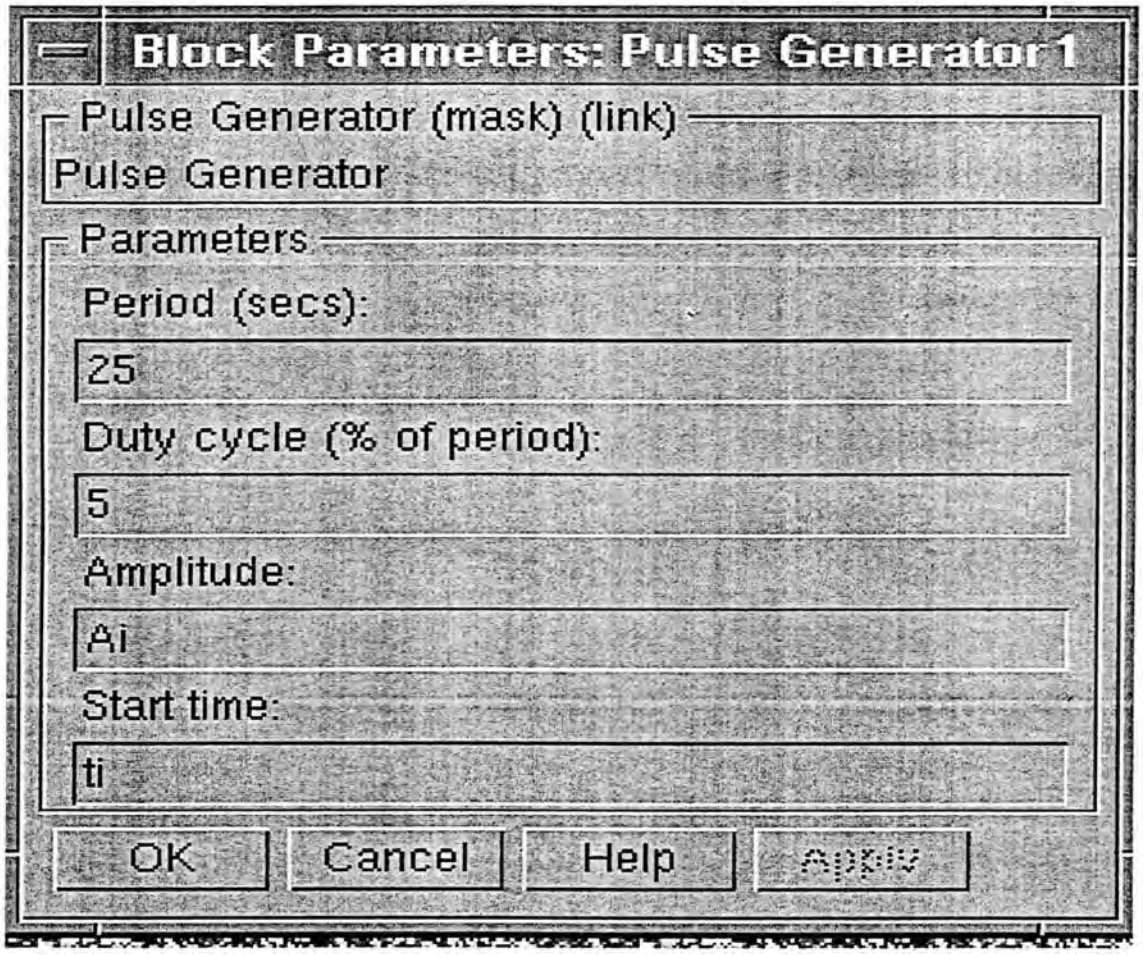

FIGURE 5.13: Simulation Pulse Generator1

C Simulink Model of Hodgkin and Huxley Equations

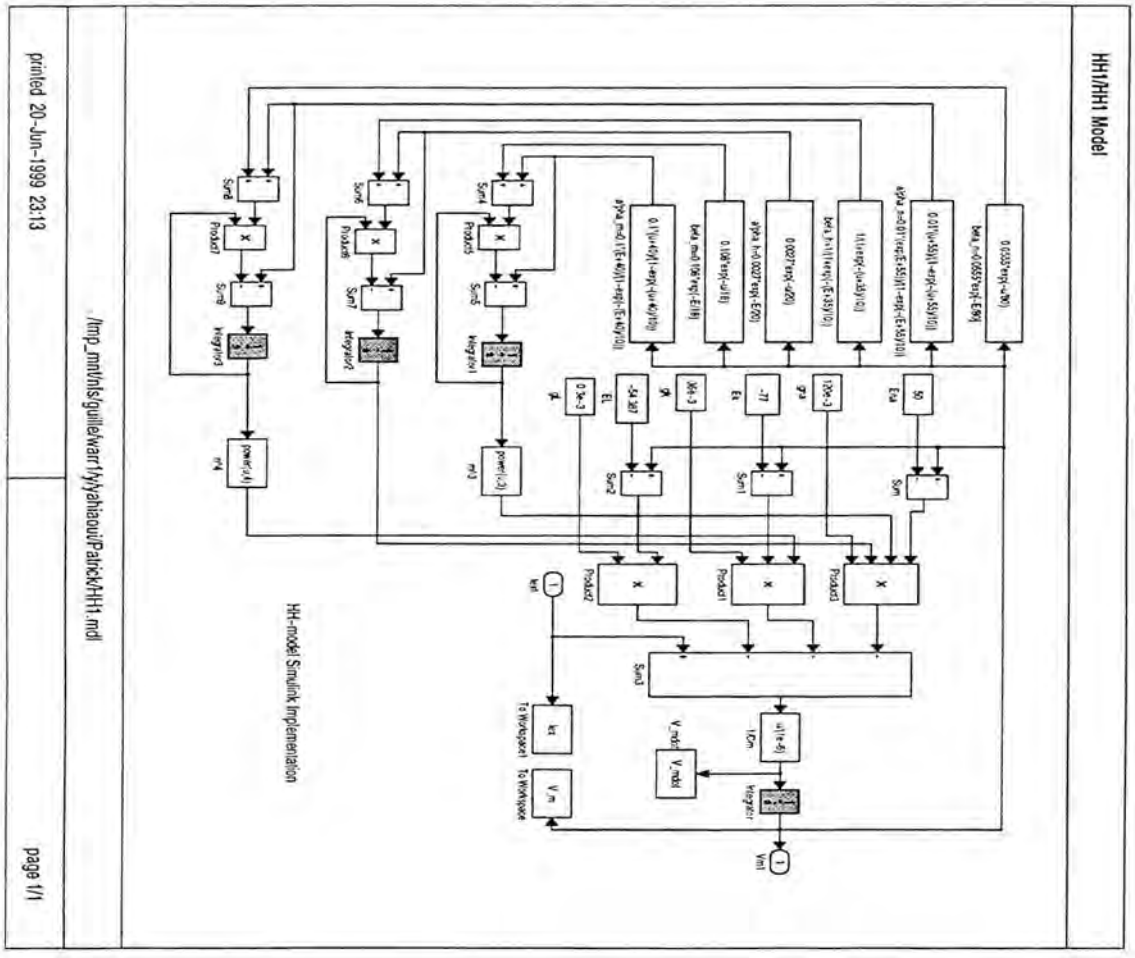

FIGURE 5.14: Simulink implementation of the HH-model

D Simulink Implementation of the BLS-model with Dual Stable focus Equilibrium Points

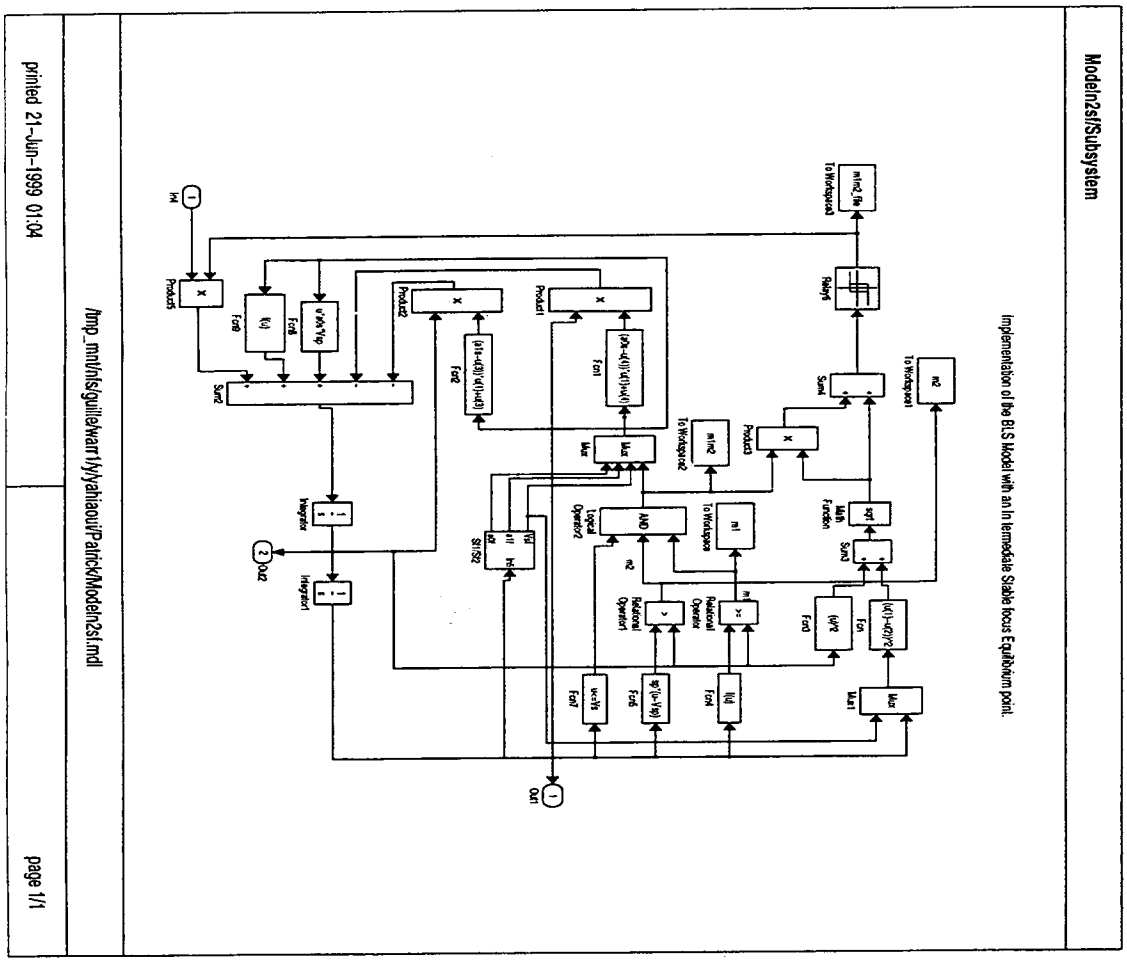

FIGURE 5.15: Simulink implementation of the BLS Model